DESIGN, DEVELOPMENT AND PLANNED PROOF OF CONCEPT FOR A GATE FUNCTIONALIZED DRUG DELIVERY METAL ORGANIC FRAMEWORK (MOF)

by

TYLER NUNGESSER

(Under the Direction of RICHARD MORRISON)

ABSTRACT

Metal Organic Frameworks (MOFs) and their vast array of topologies, constitutions and applications have incurred great interest over the past two decades. Many areas of chemical research have been impacted in the potential that MOFs bring to the table. These include gas storage and separations, chemical catalysis, endeavors in the removal of harmful and toxic environmental chemicals, magnetics, and drug delivery. Herein, a MOF has been directedly developed towards a material that is able to encapsulate biologically active molecules and subsequently release this cargo upon irradiation at 365nm LED light. This designed MOF is to act as a proof of concept for the utility of a photolabile gated or door moiety which has, to my knowledge, not been explored or unobserved in any light-mediated drug delivery MOF.

INDEX WORDS: metal organic framework (MOF), drug delivery, photoactive MOF,

DESIGN, DEVELOPMENT AND PLANNED PROOF OF CONCEPT FOR A GATE FUNCTIONALIZED DRUG DELIVERY METAL ORGANIC FRAMEWORK (MOF)

by

TYLER NUNGESSER

Bachelor of Science, Christopher Newport University, 2015

A Dissertation Submitted to the Graduate Faculty of The University of Georgia in Partial Fulfillment of the Requirements for the Degree

DOCTOR OF PHILOSOPHY

ATHENS, GEORGIA

2021

DESIGN, DEVELOPMENT AND PLANNED PROOF OF CONCEPT FOR A GATE FUNCTIONALIZED DRUG DELIVERY METAL ORGANIC FRAMEWORK (MOF)

by

TYLER NUNGESSER

Major Professor:	Richard Morrison
Committee:	Robert Phillips
	Steven Wheeler

Electronic Version Approved:

Ron Walcott
Vice Provost for Graduate Education and Dean of the Graduate School
The University of Georgia
August 2021

DEDICATION

Helen Ritter, my late great grandmother who supported me during my time in Athens pursuing my doctorate and continues to do through her memory. Jeffrey Carney who prepared me for graduate school and has a passion for organic chemistry unrivalled by anyone I know. My parents Brett and Michelle Nungesser who did everything in their power to make sure I was able to pursue the path in my academics that I had chosen.

ACKNOWLEDGEMENTS

To the many undergraduates, Emmerson, Taylor, Anya, Xena, Trey and Rueben who have aided in the chemical synthesis of the products used in the MOF synthesis. To my advisor Dr. Richard Morrison, who encouraged and supported me through this project. To my knowledgeable and supportive committee, Dr. Robert Phillips and Dr. Steven Wheeler who have offered advice and guidance throughout this project. Dr. Ian Walton whose discussion about MOF synthesis and characterization with me directed me in the final months of this project. Dr. Eric Formo who helped with visualization of our MOF products under transmission electron microscopy.

TABLE OF CONTENTS

Page

LIST OF FIGURES

Page

LIST OF TABLES

Page

LIST OF SCHEMES

Page

CHAPTER 1

INTRODUCTION

1.1 MOF background and general anatomy

Over the course of the past two decades, metal organic frameworks (MOFs) have firmly established themselves as an integral family in the world of materials chemistry. Their potential, that stems from possessing vast arrays of topologies and constitutions, has been described before to be limited only to a chemist's own thinking.[1] From the myriad of ways to construct MOFs arises a long and growing list of applications for these frameworks. As the designer, a chemist chooses deliberately which components and what qualities those components must have to produce a material with desirable yet effective qualities. Metal organic frameworks exist at the articulation of organic and inorganic chemistry, being comprised of inorganic nodes chelated into an ordered porous network by di-carboxylic acid organic linkers. Individually, the identity of these two components can influence the framework pore size, geometry and chemical behavior.

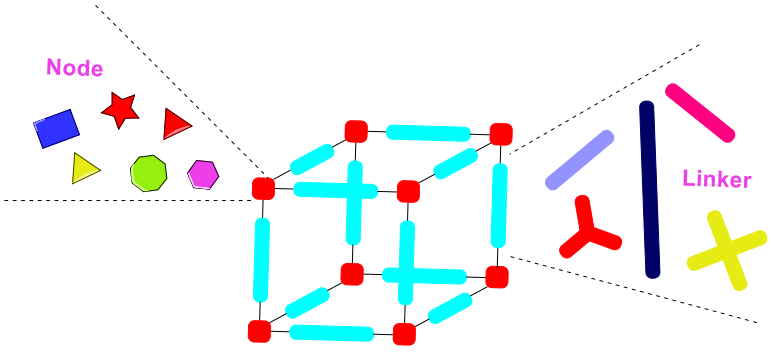

Figure 1. Cartoon representation of a metal organic framework pore and its components; the inorganic node and the organic linker. Expressed in the figure is the myriad of identities both the node and the linker can take, thus presenting a vast number of possible combinations, and therefore a vast number of geometries and chemical compositions.

At their earliest function and most basic constitution, MOFs were synthesized to maximize pore size without sacrificing structural integrity to store gasses such as hydrogen, nitrogen or oxygen.[2] Imparting chemical activity to a MOF most often involves functional group decoration along the organic linker, although, the metal inorganic node has been observed to participate in reactivity as well.[3] Loosely analogous to the active site of a protein, the function of a MOF pore is directly reflected in its structure and composition. Therefore, with a theorized function and mechanism of action hypothesized, a structure can be directedly designed.

1.2 MOFs in drug delivery

Many strides have been made in the utilization of MOFs in cargo delivery. Given the highly porous nature of MOFs and their relatively large inner surface area per gram, MOFs are an exceptional candidate for a drug delivery material. There has been one reported MOF utilized in clinical trials to date, further enhancing the rising importance of investigation in drug delivery MOFs.[4] Largely dependent on the length of the organic linker, typical MOF pore sizes can accommodate small molecules such as ibuprofen and 5-fluororacil while some systems are able to contain larger molecules such as doxorubicin.

Design of a drug delivery system requires consideration of three important factors 1) composition 2) mode of action and 3) post synthetic modifications. Beginning with the discussion on composition, it is worthy to note that there are arguably more restrictions here than in the composition of MOFs designed for other applications. The issue of MOF composition lends itself to the fact that following drug delivery, the MOF should be broken down into its primary components allowing for its removal from the body.[5]

Therefore, both the inorganic metal node and the organic linker must not individually or together pose threats of toxicity. The desired linker needs to also show no reactivity to the environment other than that of the desired modality that is supposed to result in cargo release. The materials the MOF is comprised of should be passed through the body renally or processed in a metabolic pathway ultimately leading to the exodus of those materials from the body.

Choice of the specific organic linker can be generalized to be between compounds that are endogenous or exogenous.[5b] Not surprisingly, most investigation in this area has been performed on exogenous linkers. These compounds generally act as more rigid linkers and can also be manipulated and functionalized. It is advantageous to utilize a rigid linker in a MOF as it offers regularity in pore size and shape while also offering structural integrity. There has been some investigation on using endogenous linkers such as different amino acids, but there is still much work to be done in this area. The identity of the metal inorganic node importantly determines the geometry of the MOF pore while also determining the chelating strength of the organic linker and thus the overall structural integrity.[7d] The identity of the metal used in a drug delivery MOFs however should be biologically innocuous. For example, metals such as iron and zirconium are largely chosen over metals such as chromium. A visual representation of how a metal node imparts MOF pore geometry is presented in Figure 2.

There are two modes that are utilized in order to take advantage of the drug delivery abilities of a MOF and can be generalized as passive delivery and stimuli-responsive delivery. Passive delivery relies on the deconstruction of the framework and subsequent delivery of cargo while the MOF exists in biological media. Stimuli

responsive delivery encompasses any system in which the MOF is acted upon by an external stimulus to initiate release in a controlled manner and on specific timeline. Early in the history of drug delivery MOFs, many systems where investigated that were passive delivery systems. Following an influx of knowledge and innovation into this area, drug delivery has been accomplished via thermal regulation, electromagnetic irradiation, and pH regulation to name a few.

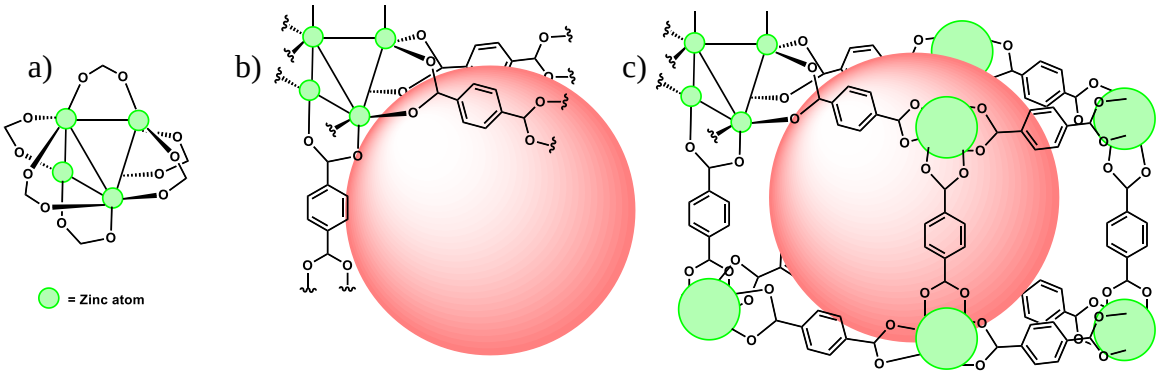

Figure 2. Depicted is a) a tetrahedral zinc node surrounded by the beginnings of six carboxylate linkers. Building in complexity to aid in visualization, the node is then seen in the context of the pore (red sphere) as it begins to take shape in b). This stems ultimately from the angle at which the carboxylate linkers extend from the tetrahedral node. In c) the organic linkers have been extended completely and terminated at each zinc node that exists at the corner of the cubical pore, thus completing the three dimensionality. It is important to understand the impact that the inorganic node geometry has on the overall pore structure of a MOF. In doing this, a MOF can be theorized, designed and developed from the very fundamental components of its composition.

By and large pH responsive MOFs take advantage of the aforementioned passive deconstruction of the MOF framework, thus leading to cargo release. Very generally decreasing the pH of the media that the MOF is suspended in will fasten the rate at which the framework is broken down. Several factors will modulate this and there are exceptions to this[6;] however, the overall trend is that more acidic environments lead to MOF decomposition. It has been theorized mechanistically that during this process, the carboxylic chelation is competitively re-protonated in more acidic environments thus resulting in the disassociation of the chelating moieties from the metal node. In the

exception what is observed in high aqueous pH ranges is that the hydroxide anions compete with the carboxylate chelators for coordination sites on the metal node.

Apart from the pH of the solution, a major variable in the extent of this process is the strength of the cationic nature of the metal center of the inorganic node. An example of this would be comparing the relative cationic strength of a 2+ zinc metal center and a 4+ zirconium metal center. Zinc MOFs are well documented and are some of the most pioneering materials that have been studied in MOF history.[7] Exhibiting high inner surface area and a relatively strong framework to its predecessors, MOF-5 is constructed from terephthalic acid and Zinc nitrate and was featured by Dr. Omar Yaghi in gas adsorption studies in the early 2000's.[7b] A well-documented limitation of MOFs utilizing zinc in the node however, is that the framework is readily hydrolyzed in the presence of even small amounts of moisture.[8] Contrasting this to a MOF utilizing zirconium in the metal node, the analogous framework, UiO-66 synthesized from terephthalic acid and zirconium chloride it has been observed that in neutral aqueous media, the framework is relatively much more robust.[9] Therefore, and unsurprisingly there have been many drug delivery MOF systems derived from zirconium given its biological inertness and exception stability to biomimetic environments. Commonly seen MOFs include UiO-66, the zirconium analog of MOF-5, and it's close relative UiO-67 which differs only in using 4,4'-dibenzyldicarboxylic acid as the organic linker instead of terephthalic acid slightly increasing pore size.

1.3 Filling a Gap in the Literature

A well-documented family of zirconium-based drug delivery MOFs utilize the linker azobenzene-4,4'-dicarboxylic acid and release their cargo upon irradiation at 365

nm light.[10] Under ambient light conditions the diazo linkage exists in the trans conformation and so when implemented into a MOF, this linker acts effectively has a linear strut resulting in typical zirconium MOF pore shape and size. However, under irradiation at 365nm light, the diazo linkage in the MOF linker undergoes isomerization to the cis conformation which results in removal of the carboxylic chelator functionality from the metal node. This isomerization effectively opens the MOF pores thus resulting in the disassembly of the framework and subsequent release the cargo.

In order to set this research apart, a MOF derivative of UiO-67 has been designed featuring a "gated" framework complete with a photolabile door moiety. The design of this MOF is based on the theory that the small molecule of interest will be confined within the MOF pore and then released at a specific time under controllable conditions. One feature of this design also includes the ability for the MOF cargo to be released while keeping the framework itself assembled. To date, there have been no examples in the primary literature of a drug delivery zirconium-based MOF utilizing a gate-opening release mechanism mediated by light. My hypothesis is that the MOF designed and synthesized herein will possess the ability to be charged with a biologically active small molecule of interest which will remain sequestered within the framework until light stimulates the release of the cargo through the photolysis of the gate door moiety.

CHAPTER 2

LITERATURE BACKGROUND

2.1 History of Drug Delivery MOFs

In 2006, Férey et al. presented one of the first pioneering examples of MOFs being utilized as a drug release material. In this system, a chromium-based MOF was constructed with either terephthalic acid (MIL-101) or 1,3,5-benzenetricarboxylic acid (MIL-100) and was charged with ibuprofen post-synthetically. An important initial take-away from the utilization of different organic linkers is seen in the carrying capacity difference inherent to using two different linkers. As one of the first instances of these materials being loaded with small molecules of interest, an inherent question in this study was an inquiry into the loading capacity of MIL-100 and MIL-101. Depicted in Figure 3, it was observed that MIL-101 had a larger pore size (~12.6 Å) and thus a greater inner surface area exhibiting a Langmuir adsorption of nitrogen of 5510 m^2/g. In contrast, MIL-100 exhibited a nitrogen adsorption of 3340 m^2/g with a pore size of ~9.7 Å. This difference in inner surface area was reflected in the loading capacity studies where it was observed that MIL-101 was able to hold 1.376 g ibu/g MOF while MIL-100 held only 0.347 g ibu/g MOF. Following loading these materials with ibuprofen, the release was then analyzed (Figure 4). It is important to note that the mode of delivery was achieved

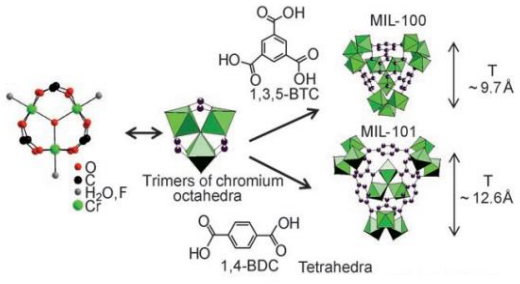

Figure 3. Node shape and pore size comparison between MIL-100 and MIL-101. Pore size was found to be directly related to nitrogen adsorption capacity.

passively through diffusive action and as the MOF hydrolyzes in the biomimetic fluid used in the release studies. Over three days MIL-100 release 100% of the loaded ibuprofen with 80% being delivered after 1.5 days. It took MIL-101 six days to fully release its cargo while 90% was release after 3.5 days.[11]

Laying the groundwork in drug delivery applications in MOFs, this work compared these results to the previously studied MCM-41, a mesoporous silicate with a pore size of 36 Å. It was observed however that even though this material exhibits pore sizes larger than MIL-101, MCM-41 adsorbed quantities of ibuprofen similar to MIL-100 (~0.347g ibu/ g MOF) and also released cargo in a similar kinetic trend. The hypothesized reason for slower release observed with MIL-101 is related to the increased π -π stacking inherent to the larger pores to this MOF. They theorized a larger pore increased the number of aromatic rings per pore, thus allowing for an increase of electronic interactions within each pore with the benzene rings of the ibuprofen molecules. It could be argued that for this reason, implementing hybrid organic/inorganic materials as drug delivery materials has increased the carrying efficiency of frameworks with similar or smaller pore sizes.

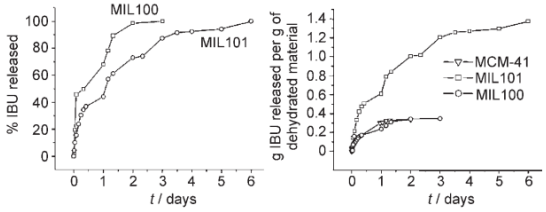

Figure 4. Data comparing the loading capacity and release of ibuprofen between MIL-100 and MIL-101. The release study also shows the important comparison in the release of ibuprofen between the two MOFs and already establish drug carrying material MCM-41.

This work was expounded later by the same group synthesizing MIL-53(Cr) and MIL-53(Fe).[12] These materials are analogous to MIL-101 in that they are synthesized using terephthalic acid and metal oxide clusters containing either chromium or iron, however modulation of synthesis conditions produce three-dimensional

frameworks that posses' one-dimensional channels. The nature of one-dimensional channels allows for inherent flexibility in these frameworks without any observed bond breakage as depicted in Figure 5. The pores of chromium MIL-53 was observed to expand from 7.58 Å to 13.04 Å. In regard to drug delivery, the flexibility in the framework imparted a much slower ibuprofen delivery rate than the analog MIL-101. It was theorized that because the pores of these breathable materials are able to dynamically accommodate different numbers of ibuprofen molecules, the pores relax as the number of cargo molecules decrease. This optimizes the pore size and sequestering capability as the drug is delivered. The aforementioned π -π linker-guest molecule interactions play a role in aiding in keeping molecules contained longer as pores shrink thus resulting in a longer release time. It was observed that both derivates of MIL-53 released 100% of their cargo only after 18 and 21 days, chromium MIL-53 and iron MIL-53 respectively. The nature of the drug release of this system can be described as passive diffusion and framework disassembly. Importantly, these finding highlight the ability for MOF containing the same components to possess drastically different qualities as drug delivery systems.

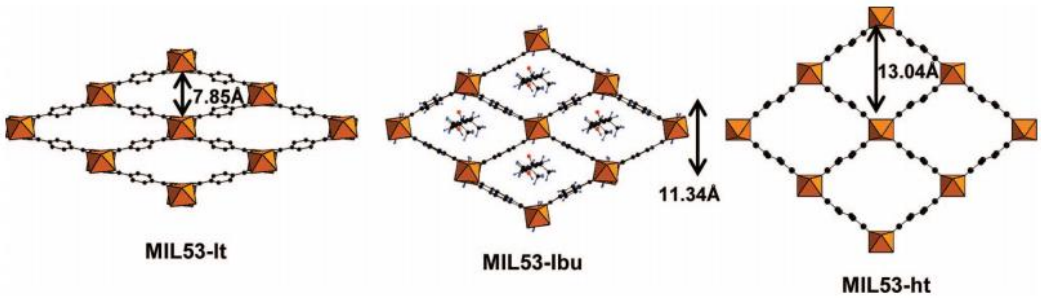

Reprinted with permission from J. AM. CHEM. SOC. VOL. 130, NO. 21, 2008. Copyright 2021 American Chemical Society
Figure 5. Visual representation of the "breathable" capability of the one-dimensional pore system of MIL-53 (Cr) and the ability for this material to expand to accommodate ibuprofen guest molecules. lt=low temperature or "hydrated state" ht=high temperature (dehydrated state).

2.2 Non-covalent drug delivery

The nature by which MOFs encapsulate their cargo can be generalized into two groups, non-covalent drug delivery and covalent drug delivery. As in the examples mentioned above and in many developed systems to date, non-covalent drug delivery involves the loading of a guest molecule into a MOF under the influence of only electrostatic or Van der Waals interactions. The efficiency of this loading can vary depending on the electronics of the organic linker, the guest molecules, the metal node and the solvent. By and large, if the goal of a system is to encapsulate the maximum amount guest molecules possible, it is advantageous to functionalize the organic linker with electron rich anchoring groups, such as amine or hydroxyl groups. In the following examples, it has been observed how decoration along the MOF linker can greatly enhance drug loading capabilities.

In 2012, Maurin and coworkers investigate how different functionalization on the organic linker influence the caffeine cargo loading capabilities of ten different derivatives of their chosen organic linker.[13] This work highlights an iron derivative of MIL-88B, a breathable MOF constructed from oxo-centered iron (III) trimers and terephthalic acid. In this work, the four positions (4X) along the benzene ring of the terephthalic acid linkers were substituted with various polar and non-polar groups. These included X= 4H, $2CF_3$, $2CH_3$, 2OH, $4CH_3$, 4F, $1CH_3$, $1NH_2$, $1NO_2$ and 1Br as seen in Figure 6. Experimentally and computationally,

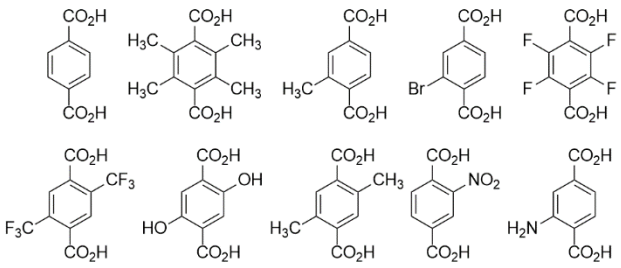

Figure 6. The ten organic linkers used by Maurin et al. in their SAR study on how functionality along the organic linker influences the carrying capacity and retention ability of cargo carrying MOFs.

they found that the more hydrophilic -2OH and -NH_2 groups allows for a greater uptake of caffeine molecules than any of the other terephthalic acid linker derivates. Interestingly and perhaps counter-intuitively, they also found that a slight increase in efficiency was also observed with the addition of mono- di- and tetra substituted methyl groups, theorized by the increase of Van der Waals interactions. This and resulting work will aid in the development of robust models for predicting the drug loading capabilities of current unanalyzed MOFs as well novel MOFs that are currently being designed.

2.3 Covalent Delivery MOFs

MOFs that are constructed with or derivatives of their cargo are described as covalent delivery MOFs. These frameworks can utilize the cargo to be delivered as the organic linker, or contain the cargo covalently bonded to the surface of the MOF as in most targeted delivery systems. As this is not the method by which I have designed my MOF system, elaboration on this MOF type will remain brief.

A very noteworthy example of not only a covalent delivery MOF, but also an example of a system that utilizes an endogenous organic linker was reported by Serre and coworkers in 2010.[14] In this innovative example, the organic linker utilized was nicotinic acid complexed together into a framework of iron (III) trimers. This MOF, termed BioMIL-1, relied on the natural decomposition of the framework structure to accomplish the nicotinic acid drug delivery. As an initial step into this direction, this work produced a semi-robust material, observing complete release of organic linker and full degradation of framework in about one hour. Further investigation into works such as this look to produce systems that deliver cargo more efficiently and controllably.

2.4 Light Mediated Drug Delivery

One of the most commonly investigated light mediated drug delivery MOFs are based off azobenzene-4,4'-dicarboxylic acid. As described above, the advantage of utilizing this linker is the ability to control the time of cargo release. Until now, all examples given have been systems that release cargo spontaneously either through diffusion or MOF disassembly.

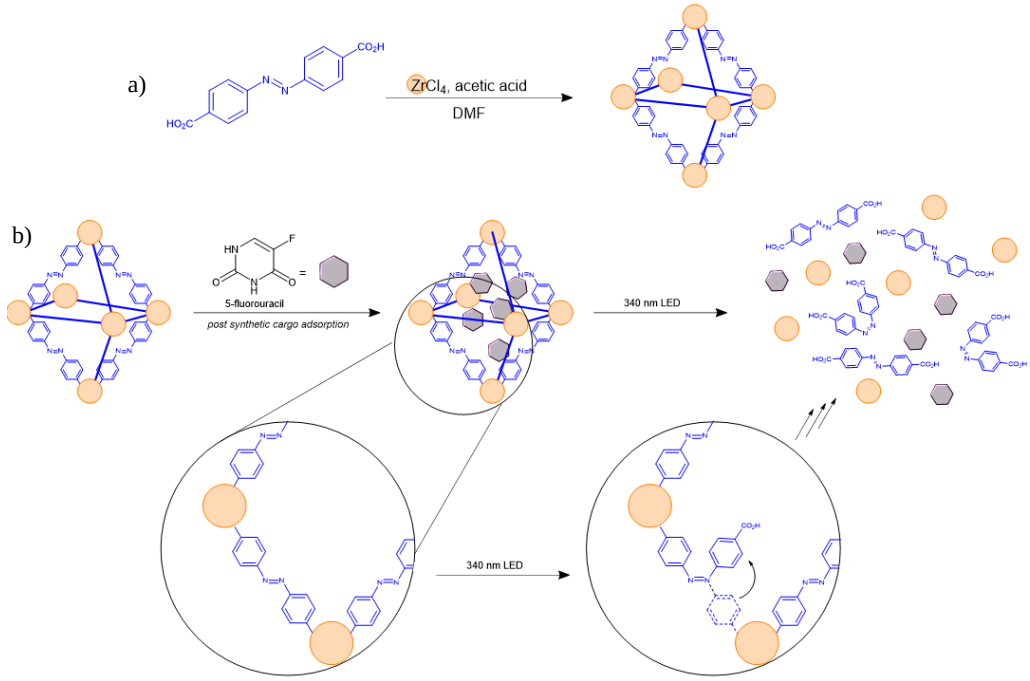

Figure 7. a) UiO-AZB synthetic scheme. b) visual representation of how a UiO-AZB MOF pore is loaded with cargo post-synthetically, and then the nature of pore deconstruction and subsequent cargo release. When submitted to irradiation at 340 nm, the azobenzene linkers undergo an isomerization from the E confirmation to the Z confirmation. This effectively pulls the chelating carboxy group from the zirconium nodes which leads to MOF disassembly.

When utilized in a zirconium-based framework, so called UiO-AZB, the produced framework exhibits robustness to biomimetic solvents, thus enhancing the impact of being able to control drug release with external stimuli. The first reported case of this MOF being illustrated to take advantage of this design came from Morris and coworkers in 2012.[15,10] In this work, UiO-AZB was tested in post-synthetic loading condition with caffeine, ibuprofen, and the dye Nile red. It was reported that ibuprofen

was able to be loaded in 38.2 wt% while caffeine was loaded in 3.4 wt%. This observation supported their theory of a greater ibu loading given the hydrophobic quality of the AZB linker. HPLC analysis of ibuprofen cargo release initially showed a small release of ibu into the solvent, however after this, no release of cargo outside of irradiation occurred, further supporting the robustness of these materials. However, upon ibu release analysis, it was observed that the ibuprofen covalently bonded to the metal node, preventing release from the MOF components. Caffeine however was unable to be sequestered under dark conditions, and therefore was concluded to be unsuitable for a controlled release using this system. This observation importantly highlights both the influence of the organic linker on the guest molecules and also the selectivity in the choice of cargo and its compatibility with the organic linker. Looking at the Nile red loading and release, this guest molecule was seen to be adsorbed in 4.3 wt%. In their first release of a molecule using this MOF design, these researchers were able to observe a nine-fold cargo release in illuminated conditions versus dark conditions. This supports the conclusion that the mechanism of release was controlled predominantly by photo-degradation.

2.5 Controllable Drug Delivery Through Mechanical Trapping

In specific support of my design for a "gated" cargo delivery MOF these next two examples demonstrate systems designed around releasing small molecules controllably with specific stimuli. These MOFs show great innovation, utilizing pendant functionalities that in one environment sequester cargo within the framework, while allowing exodus of that same cargo when presented with a different environment.

In 2015 Sada and coworkers published their first example of a thermo-responsive MOF, able to be loaded with three different small molecules, that selectively released these cargos under cooling conditions.[16] The material was designed to utilize UiO-66-NH_2 functionalized at its surface with the polymer poly(*N*-isopropylacrylamide) (PNIPAM). The amino functionalities within the MOF linker allowed not only for increased loading capabilities, but also a handle for the ligation of the polymer to the surface of the framework. The purpose of the polymer adhered to the surface of the MOF was to act as the thermo-responsive agent in the system. Under heated conditions, the polymer coils up on the surface of each MOF crystal not allowing for the delivery of the guest molecules. However, under cooling conditions the polymer relaxes and uncovers the MOF surface pore thus allowing for the diffusion of the cargo out of the framework (Figure 8). This suggests that the mechanical blocking ability of the coiled-up polymer on the surface of the MOF crystal was sufficient for the sustained sequestering of the cargo within. This also is an example of guest molecules being able to leave MOF pores diffusively after being covered. It was observed that for the three guest molecules tested, Caffeine, Resorufin and Procainamide, the highest amount of cargo release at heated conditions was ~20% which remained unchanged for seven days. However, under cooling

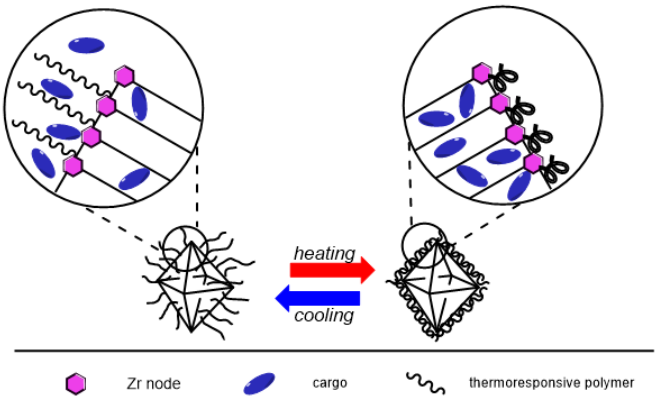

Figure 8. Sada and coworkers thermo-responsive UiO-66-NH_2 MOF. The polymer PNIPAM is chelated to the surface of the MOF particles via amine functionality. In heating conditions, the polymer coils up on itself physically blocking pore openings thus preventing cargo exodus. In cooling conditions these polymer strands relax, opening the surface pores allowing cargo release.

conditions,70-90% release was observed only after 24 hours and 90-100% release was observed after four days.

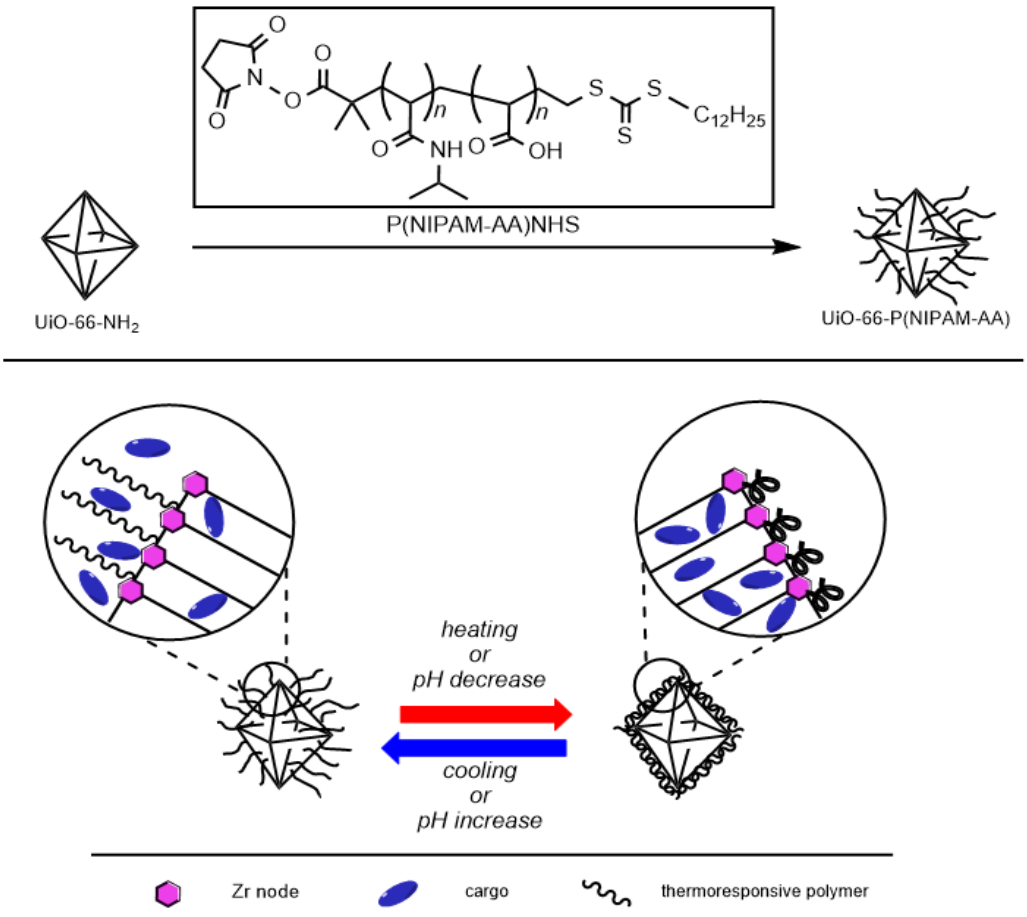

Figure 9. Sada and coworkers and their drug delivery MOF system that is both pH and thermo-responsive. In this example, the addition of the acrylic acid to the polymer synthesis imparts pH responsive qualities. At low higher temperatures or if the pH of the environment decreases, the surface polymer coils up and blocks the surface pores as in the previous example. In cooler temperatures or at slightly higher pH the surface polymer relaxes allowing for the pores to be uncovered.

Perhaps most interestingly, this system was tested and confirmed to be reversible. Submitting this system through cooling and heating cycles revealed that cargo delivery was able to be tuned on and off.

Four years later this same group published a work highlighting the development of a similar bi-modal system (Figure 9).[17] This material was based off UiO-66-NH_2 as well, however utilized a surface polymer that was pH responsive as well as thermo-

responsive. During the synthesis of the polymer to be used in surface modification, the researchers co-polymerized with acrylic acid creating poly *N*-isopropylacrylamide acrylic acid, or (P(NIPAM–AA)). In this study, Procainamide was loaded into the framework under relaxed polymer conditions and the release was observed under high or low pH. Under a low pH of 4.01 and at 40º C the acrylic acid doped surface polymer aggregated on the surface of the MOF crystal, not allowing for cargo delivery even after seven days. However, the opposite was observed for a relative higher pH. At a pH of 6.86 and 40º C, 90% cargo delivery was observed after six days. Also, much like in this groups first thermo-responsive example, this material was also able to be switched on and off based on its environment, observing release at near neutral pH, with no drug delivery occurring at lower pH.

These two examples provide strong evidence for the applicability of a "door opening" cargo delivery system. Showing that small molecules are able to be sequestered within MOF pores by mechanical blocking and then subsequently release following an opening of those pores. Moving forward, the specific theory behind the design and application of such a drug delivery system will be elaborated upon.

2.6 Concerns surrounding UV light activated drug delivery

Drug delivery systems activated by light have been investigated greatly and offer high control over on-demand cargo release. Drug delivery systems that utilize this stimulus to instigate cargo release take advantage of either the indirect or ambient exposure of the surrounding light, or controlled and artificially sourced electromagnetic irradiation of very specific wavelengths, ranging from 2500nm to 380nm. Light activation by nature is non-invasive, it offers high spatial resolution and temporal control

usually unobserved in other stimuli and is also convenient and easy to use.[18] Wavelengths in the red color range in the electromagnetic spectrum (600-650 nm) and in the near infrared (NIR) (650-950 nm) region more easily penetrate biological surfaces ranging from 3-8 millimeters in depth.[19] This is due to the lessened scattering and absorption of the light waves by water and the various tissues that comprise the skin. Photodynamic therapy (PDT) is one well-studied method of light stimulated skin cancer treatment that is already applied clinically. PDT treatment utilizes waves in the red zone of the light spectrum to activate photosensitizers within the tumor releasing reactive oxygen species thus reducing the viability of the tumor cells. Development of novel phototherapies can greatly benefit from the advancements made in the already commercialized PDT.

One significant drawback of utilizing light as a drug delivery stimuli however, is the low penetration depth of ultra-violet light, limiting the applications of this area of the light spectrum. Nevertheless, UV light has been utilized in drug delivery systems that are used on the surface of the skin, or in systems where the drug carrier circulates in blood vessels close to the body surface.[20] Furthermore, many light-activated drug delivery systems operate within this wavelength region, utilizing commonly used chemical functionalities that are cleaved or influenced by the UV region, one of them being azobenzene linkages, as discussed in the previous chapter. There are a multitude of light sensitive motifs utilized in the advancement of drug delivery, many of which are structurally manipulated in order to tune the wavelength at which they are activated.[21] One of the most commonly used and investigated is the o-nitrobenzyl ether (oNBE) and the derivates thereof. Much work has been accomplished on this family of ethers in the area of protection group chemistry, however the interest in using this functionality has

shifted to using the oNBE as a pro-drug for many drug delivery applications.[22] Because of this, the biocompatibility of the oNBE and the product of its photocleavage has been scrutinized. It is well documented and established that the product of the photocleavage of this motif is an o-nitrosobenzaldehyde. Concerns for the chemical toxicity attributed to the byproduct of cleavage as well as the phototoxicity concerns in the utilization of UV light cannot be ignored, however, oNBEs still offer a powerful way to investigate drug delivery systems in proof-of-concept situations.

One important way researchers have been able to apply UV light to the activation of oNBEs without having to account for penetration depth is in the application of upconversion nanoparticles (UPCNs). UPCNs are utilized in nanotechnology and enable the conversion of longer wavelength emissions to shorter wavelength emissions. These nanoparticles are doped with lanthanide metals and through specific selection of a particular dopant, specific modulation of electromagnetic waves can be achieved.[23] By and large, NIR wavelengths are able to be upconverted to, shorter NIR, visible light, and UV light (Figure 10). It could be envisioned that in conjunction with a drug delivery system that requires UV light to function, UCNPs would be an efficient way to increase the application as well as the efficiency of these materials while addressing the biocompatibility concerns surrounding general UV irradiation. As this is only one option in the ways to increase the applicability of oNBEs, there is still much work to do in order to apply them to *in vivo* applications

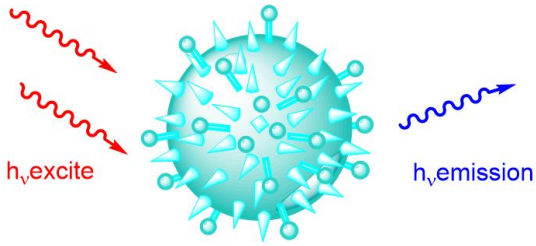

Figure 10. Cartoon depiction of how up-conversion nanoparticles function. Based on the lanthanide doped chemical make-up of the core nanoparticle, excitation wavelengths (usually IR) are converted to shorter wavelengths which are then emitted directly from the particle.

and let alone a clinical environment. All in all, the o-nitrobenzyl photolabile group is a powerful tool in the discovery of light stimulated drug delivery applications and remains a very viable candidate to be used in proof-of-concept applications.

CHAPTER 3

THEORY

3.1 Design Theory

There is evidence in the literature supporting the importance for the discovery of novel methods by which drug delivery MOFs mechanistically deliver their cargo. As one example, it could be advantageous to deliver cargo controllably, while keeping the overarching framework intact. In the breathable MOF examples mentioned in the previous chapter, cargo was able to diffuse out of the MOF matrix without a change to the pore constitution, however in these cases the delivery of the cargo was not controllable and relied on passive delivery over time. Development of drug delivery systems that release pharmaceuticals over long periods of time is advantageous as it offers possibilities into new systems that are able to be administered once and then left alone. It could be suggested that materials that are able to sequester cargo with a retention time on the order of weeks or even months could be utilized in environments where a non-invasive treatment is necessary. In this case controllability would be a valuable quality in a medication such as this. To this end, it is important to also design drug delivery systems that are able to be selectively controlled.

Present in the literature also are MOFs in which the framework itself is disassembled during the delivery process. If the material is robust to biomimetic environments and can exist in the area needing treatment, these materials offer powerful control of the specific time of release and can be utilized on demand. Efforts here should

be concentrated on improving the survivability of the MOF in biological fluid. In doing this a material is produced that is able to be delivered to a specific site for treatment, while remaining unreacted, or uninfluenced in its construction, apart from the stimuli designed to release the guest molecules. One drawback of this mechanism of delivery, however, is that more concern must be given to the individual components of the disassembly. If a MOF is designed to deliver cargo with disassembly of the framework itself, then not only is the cargo being delivered to the treatment site, but the organic linker and the inorganic metal node as well. Recall here that design of drug delivery MOF should involve innocuous components that have been extensively tested for their toxicity concerns.

Efforts in the research described in detail later in this document surround the postulate that a robust MOF can be designed to deliver the cargo within its pores under irradiation of a specific wavelength of light while remaining largely unchanged in its construction. Theoretically, if loaded with an anti-cancer therapy drug, a system described as such would be able to be implemented in conjunction with the enhanced permeability and retention (EPR) effect.

3.2 Delivery Theory

The EPR effect has been well documented and investigated mostly in the realm of nanomedicine. Researchers working on the development of novel therapeutic nanoparticles have relied on this phenomenon before.[24] The EPR effect can be described as the accumulation and intertumoral distribution of nanosized particles within a solid, relatively advanced stage tumor due to gaps in the lining of the blood vessels surrounding the tumor site, visualized in Figure 10. To take advantage of this effect, a nanomedicine

is injected intravenously and is then allowed to circulate throughout the circulatory system. During this time, the nanoparticles are susceptible to tagging from the host immune system and subsequent excretion from the body. During circulation within the body, the nanoparticles are able to diffuse across the lining of blood vessels as mentioned before (Figure 11). It is worth mentioning here that while particles can diffuse into the tumor microenvironment, they can also diffuse in the opposite direction as well depending highly on the composition of the tumor site. The tumor microenvironment is highly complex and specific, varying with the type of cancer and with different patients. While the EPR effect has been heavily debated, it has been observed that within humans, it is possible for nanosized medicines to accumulate within tumor sites.[24]

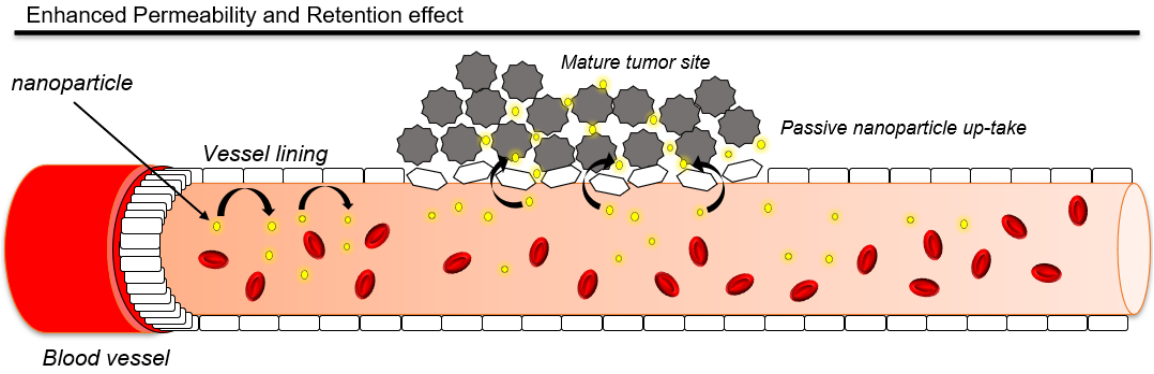

Figure 11. A visual description of the enhanced permeability and retention (EPR) effect. This phenomenon takes advantage of the micro gaps that are present within the cell wall lining of blood vessels that surround advanced staged tumors. These small gaps give the enlarged tumor site some degree of permeability, and thus allows for the diffusion of nanoparticles in and out of the tumor. EPR relies on passive diffusion, as the nanoparticles circulate through the bloodstream. The theory is that once the nanoparticles are taken up into the tumor site, they are then able to administer therapeutics to this site.

It is important to note here that although utilization of the EPR effect is a major driving force in the development of novel nanomedicines, this effect is relatively weak, typically only allowing for 5-10% uptake efficiency. A method to improve this percentage lies in the utilization of a specific targeting ligand decorated on the surface of the drug carrier that will direct the nanoparticles to the tumor cells specifically.

Implementation of a targeting ligand in context of the research described herein will be presented in a later chapter. Implementation of a MOF drug delivery system would require the qualities described previously. If a robust enough framework is synthesized, then the MOF would be able to persist circulation within biological fluid. Design of a release mechanism unable to be triggered within biological medium would then be the goal of most importance.

3.3 Release Theory

The hypothesis formulated around the gated MOF that will be described herein is theorized to work in accordance with the examples published by Sada and coworkers showcasing MOF systems that allowed control over the delivery of cargo in response to the opening and closing of pores by an actuating surface polymer. The ability of cargo to be delivered utilizing a door opening mechanism has yet to be investigated in the primary literature. In this work, an o-nitrobenzyl ether (oNBE) protecting group integrated into the organic linker of the proposed MOF is postulated to act as an entity that can mechanically block cargo and prohibit its exodus from the framework once trapped inside. As seen from Sada *et al.* this mechanical trapping of guest molecules has been observed and reported before.[16,17] As a proof on concept, this designed modality could be the first example of a MOF drug delivery material that delivers its cargo only following

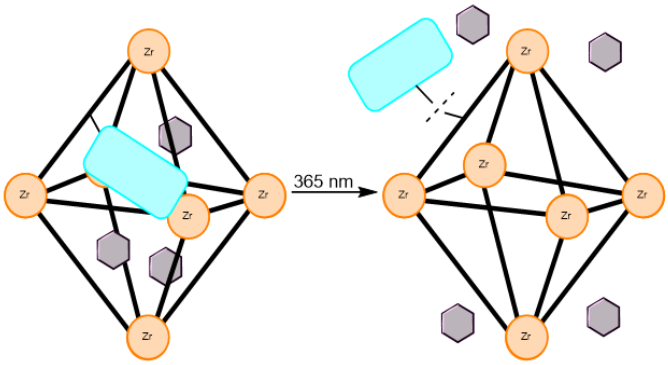

Figure 12. A reductive visual of the theorized function of the gate-functionalized MOF presented within this research. The gate moiety is theorized to aid in the sequestering of cargo within the MOF pore. Upon irradiation at 365 nm, the gate functionality is cleaved and the pore is uncovered allowing for the cargo to be delivered from within the MOF material.

the photocleavage of a gated moiety as depicted in Figure 12. The development of a MOF material that has the potential to be loaded with cargo and the ability to keep it sequestered until a specific time and under external stimuli conditions would benefit the advancement of drug delivery metal organic frameworks. My working hypothesis is this: A novel, robust drug delivery MOF 1) can be loaded with cargo in a significant loading capacity 2) can retain the bulk of this cargo within the framework pores, sequestered by the door functionality hanging pendant from the organic linker 3) can remain unchanged in composition and perpetuate in biologically mimetic environments for extended periods of time without bulk loss of cargo 4) can under irradiation at 365nm with high specificity cleave the oNBE door moiety thus opening pores with subsequent cargo release. 5) can be irradiated in short or long intervals, releasing the respective amounts of cargo necessary for that application, highlighting the high temporal control inherent to light activated drug release mechanisms. A developed MOF material such as this successfully combining all or some of these qualities could valuably increase knowledge surrounding drug delivery MOFs and could “open new doors” to other novel and innovative drug delivery MOF designs.

CHAPTER 4

PROJECT TIMELINE AND BEGINNING

4.1 Molecular machine MOF

Through many stages of development and design optimization, a gate functionalized MOF has been synthesized. This chapter will be dedicated to a narrative describing in detail the many stages of development and optimization that were taken to arrive to the current utilized MOF design. Beginning with the first proposed MOF, the infant project which I took on initially involved a zinc-based MOF integrated with an organic linker that was proposed to act as a switchable molecular machine thread. This long, flexible organic linker contained aromatic and basic functionalities in the form of benzene and imine. It was proposed that prior to the incorporation of this linker into the MOF, the linker would be threaded with a $CBPQT^{4+}$ ring, thus forming a rotaxane interlocked compound molecule. Following rotaxane formation, this linker was to be

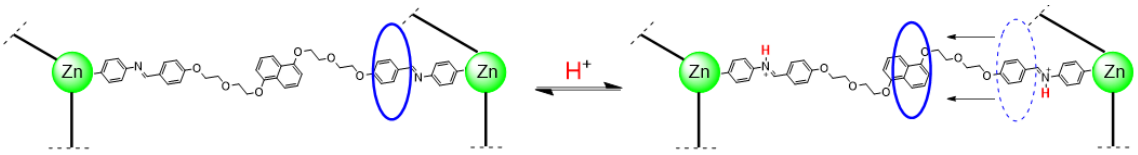

Figure 13. Mode of action theorized for the pH sensitive molecular machine organic linker that was the first attempted linker of the project. The tetra-cationic ring as seen on the right would be stationed over the basic imine site along the rotaxane thread. At lower pH, the imine nitrogen would be protonated, changing the electronic environment of the thread, and thus shift the position of the ring along the thread.

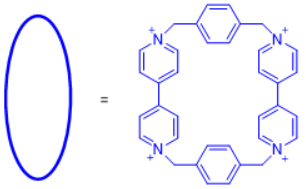

utilized in MOF synthesis. The rotaxane linker that has been described was theorized to function through the modulation of pH. At low pH, the imine functionality would be protonated which through electronic interactions, would align the

$CBPQT^{4+}$ with the aromatic station. Reversely at higher pHs, the electronic interactions of the basic imine station would place the $CBPQT^{4+}$ at the imine functionality. Utilizing the modulation of pH, the $CBPQT^{4+}$ would be able to move along the thin rotaxane thread as seen in Figure 13. Applying this organic linker system to a MOF, it was theorized to produce a framework where the pore size would be breathable but also remain controllable specifically by the stimulus of pH. It was proposed that the movement of the rotaxane ring along the organic linker thread would influence the pore diameter.

The synthesis of the components of this system involved first the construction of the $CBPQT^{4+}$ ring. This was accomplished by the reaction of 1,4-bis(bromomethyl)benzene with bis-4,4'-pyridylpiridinium. This reaction produced the $CBPQT^{4+}/4Br^-$ precursor species in quantitative yield. Following half-ring formation, an ion exchange with the synthesized $CBPQT^{4+}/4Br^-$ precursor complex was accomplished with ammonium hexafluorophosphate, producing the half ring $CBPQT^{4+}/PF_6$ in an overall yield of 81% over two steps. With a stock of the desired rotaxane ring precursor in hand, it was time to synthesize the rotaxane thread organic linker. This symmetrical rotaxane thread synthesis began with a center naphthyl station and in the form of naphthalene-1,5-diol. A bis substitution reaction of the naphthyl derivative with 2-(2-chloroethoxy)ethanol produce the elongated diol 1A. A bis tosylation of this diol was able to be accomplished in a 97% yield, preparing 2A for another bis substitution reaction with p-hydroxybenzaldehyde producing dial 3A in a 67% yield. With the desired dialdehyde in hand, the end cap synthesis was begun. The end cap in this organic linker is essential in keeping the $CBPQT^{4+}/PF_6$ threaded on the linker during the MOF synthesis. To synthesize the end cap for the rotaxane thread, methyl anthracene-9-carboxylate was

nitro functionalized at the 10 position in a quantitative yield to produce compound 4A. This nitro functionality was proposed to be the handle by which the end cap would be introduced to the previously synthesized dialdehyde following further modification. In order to obtain the desired amine functionality without disturbing the benzylic ester moiety a small optimization of reduction conditions was undertaken as shown in table 1. Initially, a tin chloride reduction was attempted, with variations thereof however, but ultimately a Pd/C hydrogenation was decided upon. Following this small optimization, the anthracene nitro derivative was then reduced in a Pd/C hydrogenation to reveal the amine a position 10 producing compound 5A in an 82% yield.

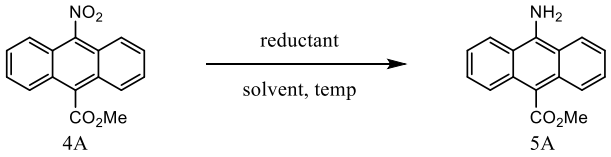

4A 5A

Entry	reductant	solvent	temperature
1	$SnCl_2$	$MeCO_2H$	80 °C
2	$SnCl_2$	EtOH	80 °C
3	$SnCl_2$	EtOH*	80 °C
4	H_2, Pd/C	CH_2Cl_2	23 °C

* denotes degassed solvent via argon balloon bubbling

Table 1. Optimization table for the reduction step in the synthesis of the end capping compound for the molecular machine MOF linker

With both the end cap and the dialdehyde rotaxane thread pre-cursor in hand, the imine formation that would form the whole organic linker was tested and optimized. At this time, the imine formation was tested without the $CBPQT^{4+}/PF_6$ ring in order to gain familiarity with the chemistry and also obtain structural conformation via NMR analysis. This analysis would then be able to be compared to the threaded linker to confirm interlocking and full formation of the rotaxane. It was found that imine formation

occurred efficiently and cleanly, producing the un-threaded and un-saponified linker 6A in a 71% yield in the presence of pyrrolidine and 4Å mol sieves. The whole synthesis can be seen in figure 13. Concomitantly to this synthesis, another MOF linker synthesis was also being performed.

Starkly different from the initial molecular machine-based MOF linker, the next linker that was investigated was theorized to function more similarly to the gated drug delivery system that was ultimately chosen. The conceptualized linker was comprised of an iminodiacetic acid backbone, that was functionalized with a 1,3,5-cycloheptatriene ring on the nitrogen within the backbone. Being decorated with a 1,3,5-cycloheptatriene ring allowed this material to be pH sensitive.

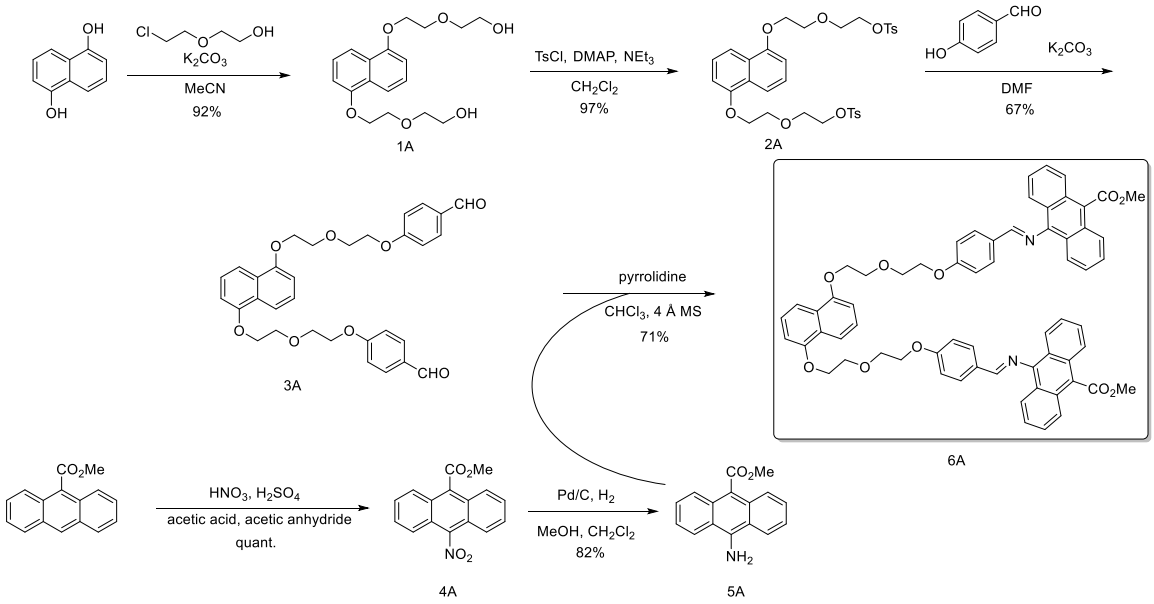

Scheme 1. Full synthesis of molecular machine MOF linker without threading of rotaxane ring along thread.

It was theorized to once integrated into a framework system, the ring along the backbone of the organic linker would act as the door within the pores of the MOF aiding in the

mechanical trapping of guest molecules in the MOF as has been previously discussed. Introduction of this MOF, once loaded with cargo, into a low pH environment would protonate the nitrogen of the organic linker backbone and thus initiate the cleavage of the cycloheptatriene ring, forming a tropylium ion in the process. As described in detail before, the cleavage of the door moiety would then open the pores of the framework and allow diffusion of the cargo out of the MOF.

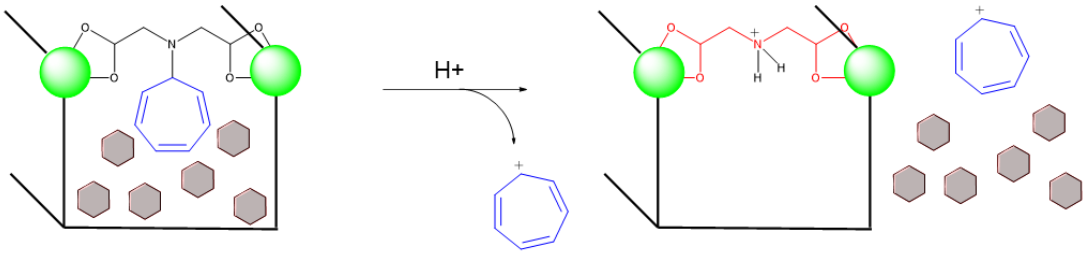

Figure 14. MOF system based off of the pH responsive cycloheptatriene functionalized organic linker. This is the first iteration of a MOF designed on the premise of a "gated" drug delivery hypothesis. The cycloheptatriene ring would act as the gate moiety in this instance, and would be cleaved off of the framework backbone when introduced to a low pH environment. Low pH would protonate the imino functionality along the backbone and the 1,3,5-cycloheptatriene ring would leave as a tropylium ion.

The synthesis of this linker began firstly with iminodiacetic acid which first required esterification before functionalization with a cycloheptatriene ring. This was accomplished with reaction of the diacetic acid and oxalyl chloride in the presence of either methanol or ethanol. Later, both dimethyl iminodiacetate or diethyl iminodiacetate were obtained commercially to expedite the synthesis. With dimethyl or diethyl iminodiacetic acid in hand, reaction conditions with tropylium tetrafluoroborate were optimized as seen in Table 2. Briefly, hard base conditions with sodium hydride were experimentally found to be most effective in the formation of the 1,3,5-cycloheptatriene ring decorated iminodiester linker precursor 1E or 2E, diethyl or dimethyl imino-backbone, respectively in an 81% yield.

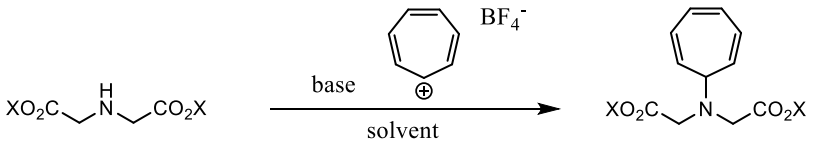

Entry	base	X	solvent
1	NEt_3	Me	CH_2Cl_2
2	NEt_3	Et	CH_2Cl_2
3	DBU	Me	CH_2Cl_2
4	NaH	Me	THF
5	NaH	Et	THF

Table 2. Short optimization of the reaction to form the cycloheptatriene decorated iminodiacetate ester.

The next step of saponification to produce the diacid linker that is able to be used in MOF formation proved difficult to optimize. The very nature of the linker I was attempting to synthesized was functional at low pH, and a necessary step in the saponification and formation of an acid functional group is the re-acidification of the carboxylate that is formed if the saponification conditions chosen are basic in nature. It was understood from an early standpoint that acidic saponification conditions would be unsuitable for this transformation and so an attempt was made to optimize a basic saponification for my starting material. Many conditions were attempted, as seen in optimization Table 3, however ultimately this saponification never yielded the diacid linker as proposed. I was determined nevertheless to obtain a structure with which I was able to attempt MOF formation.

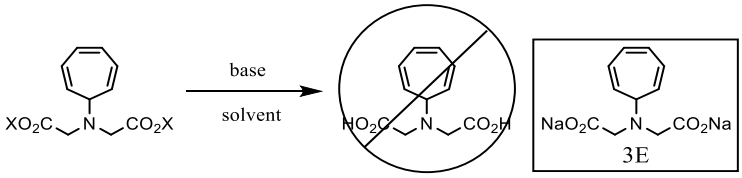

Entry	base	X	solvent
1	NaOH	Me	EtOH:acetone
2	$NaBH_4$	Me	MeOH:H_2O
3	NaOH	Et	EtOH:acetone
4	$NaBH_4$	Et	MeOH:H_2O
5	LiOH	Me	EtOH:acetone
6	KOH	Me	EtOH:acetone
7	LiOH	Et	EtOH:acetone
8	KOH	Et	EtOH:acetone
9	NaI	Et	pyridine
10	KI	Et	pyridine
11	$Ba(OH)_2$	Et	MeOH
12	$Ba(OH)_2$	Et	DMF
13	$Ba(OH)_2$	Et	THF
14	$Ba(OH)_2$	Et	1,4-dioxane

Table 3. Optimization table for the saponification reaction of either the dimethyl or the diethyl derivative of the cycloheptatriene functionalized iminodiacetate linker. Boxed entry was utilized in the formation of the dianion salt.

It is important to note here, I believe, that at this point during my career as a graduate student I had never been exposed to materials synthesis, having only ever performed small molecule synthesis with a concentration in organometallic catalysis. It is appropriate to say then that there was much learning to be done and much experience to be gained in the area of metal organic framework synthesis. Pushing along in a desire to produce MOF material, it was decided, albeit naively, to attempt and utilize the saponified disodium salt of the cycloheptatriene derivative linker 3E in a microwave-initiated MOF synthesis. While there was no precedence for this in the primary literature, scientific research by nature is investigatory, and in order to exhaust the final option I had

with this specific linker, an attempt was made to incorporate disodium salt 3E into a framework utilizing a common microwave-initiated MOF synthesis. After many attempted MOF syntheses were attempted, no characterizable material was obtained from the reaction of the disodium salt with $Zn(NO_3)_2$. Following these attempts, a revisioning of both the linker and priority was made. After spending time within the literature familiarizing myself with many developed MOF syntheses, it was apparent that while novel and innovative linker design is important, also designing it within the context of the MOF synthesis is imperative. A shift towards the prioritization of giving the framework synthesis itself the best-case scenario was made. Therefore, the proposed MOF linker should be able to withstand common framework forming syntheses. This not only includes potential acidic or aqueous environments, but also includes high temperature and pressure conditions as well. In order to move towards a system more reasonable to be successfully synthesized, a complete redesign of my organic linker was necessary. Helpfully, reading through MOFs that had been used in drug delivery applications before as well as common frameworks in general sharped the focus towards arriving at a more reasonable proposal. One major quality observed in MOF composition is that by and large, frameworks that can utilized in applications outside of the laboratory are robust and therefore are comprised of rigid linkers. At this time, both the linkers I had been attempting to synthesize and the one linker I attempted MOF formation with were flexible in nature. To be clear, there are systems that have been synthesized and utilized that exhibit flexible linker, however having first started materials synthesis just previous to this redesign, a decision was made to utilize the biggest commonalities I observed about MOF topology.

While not wildly common in MOF linkers, there is literature precedence to incorporate pendant structures along the organic linker. An important capability that arose from this research, is the ability to unveil, post-synthetically, functional groups within the organic linker that would have otherwise inhibited successful MOF synthesis. MOFs designed for catalytic purposes use this process in order to create pores functionalized to encourage unexpected reactivity, as observed in this interesting example.[25]

After much deliberation, it was decided to pursue the synthesis of a MOF organic linker derived from with terephthalic acid or 4,4'-dibenzenedicarboxylic acid. In doing this, I would be more closely following successful examples highlighted in the primary literature. It was also decided to remain inquisitive about a gated drug delivery MOF. While a pH responsive system would be logically difficult to synthesize, a move towards the development of a light driven delivery system was proposed and decided upon given the many advantages to light stimulated drug delivery. As the design began to take form, the proposed system would primarily act as a proof of concept to answer the key hypothesis, can a cargo-carrying, gate-functionalized MOF deliver cargo stimulated with a specific wavelength of light with high spatial and temporal control. Due to the drive to prove this concept, a photolabile functional group was chosen with specific cleaving conditions outside of the visible light range, and also with robustness towards anticipated synthesis conditions.

4.1 Detailed procedures for reactions within chapter 4

CBPQT^{4+} Ring

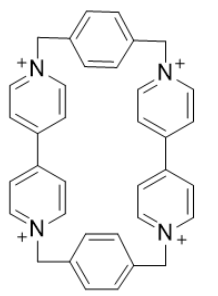

Bipy (5 equiv) was dissolved in MeCN and the solution was brought to 50 ºC. In a separate flask, the dibromo species (1 equiv) was dissolved in MeCN which was added dropwise to stirring solution of bipy over 1h while the temperature was maintained at 50 ºC. Following addition of dibromobenzyl species, the temperature was increased to 60 ºC and allowed to stir at this temperature overnight. After 16h, the reaction was filtered via buchner funnel and rinsed with MeCN (4x50mL). The crude product was taken in the next ion exchange step. The crude material from the first step was taken up in DI H_2O and heated until fully dissolved. A 1M solution of NH_4PF_6 was added dropwise and upon complete addition, the mixture was allowed to cool to 23 ºC, was filtered and then rinsed with DI H_2O (3x50mL) and dried under vacuum.

4A: Methyl 10-nitroanthracene-9-carboxylate

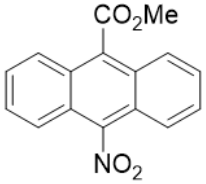

The nitro anthracene was dissolved in an acetic acid:acetic anyhydride solution (12:1) and this solution was then cooled. Once at 0 ºC, nitric acid (1 equiv) in sulfuric acid was added dropwise with vigorous stirring and was allowed to stir at 0 ºC for 1h and then was poured over ice. The resulting solid precipitate was vacuum filtered and then recrystallized in 5:1 EtOH:benzene.

5A: Methyl 10-aminoanthracene-9-carboxylate

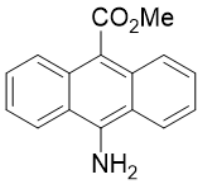

To a flame-dried flask under N_2 gas was added the Pd/C powder. This flask was then sealed and then evacuated with vacuum and then resubmitted to N_2 atmosphere (x3). Methylene chloride was then added to the powder under inert atmosphere taking care to rinse the sides of the flask to bring he Pd/C powder into the solution. Once all of the Pd/C powder was under solvent, MeOH was added. The substrate was dissolved in a small portion of methylene chloride and then added to the Pd/C mixture as well and was stirred to distribute. This mixture was again evacuated and flushed back with nitrogen (x3). On the final evacuation with vacuum, a hydrogen balloon was used instead of the last nitrogen backfill. The reaction was monitored by TLC until completed. Once reaction was complete the mixture was poured and filtered over celite taking care to not allow to bed of celite to dry. The crude reaction was the concentrated *in vacuo* and then recrystallized with EtOH.

1A: 2,2'-(((naphthalene-1,5-diylbis(oxy))bis(ethane-2,1-diyl))bis(oxy))bis(ethan-1-ol)

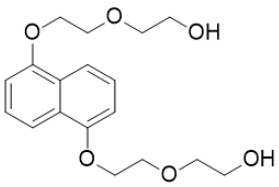

To a flame-dried flask was added the substrate (1.0 g) which was then dissolved in MeCN. To the solution was added K_2CO_3 (4 equiv). The chloroethanol (2.2 equiv) was then added to MeCN (1M) and then added dropwise to the stirring solution of substrate at 23 ºC. This reaction was then refluxed overnight to produce the desired diol. Once starting material consumption was confirmed by TLC, 20 mL of DI water was added to the reaction to dissolved potassium carbonate. The organic layer was washed with 1M HCl (2 x 10mL),

sat. sodium bicarbonate (2 x 20mL), DI H_2O (1 x 10mL) brine (1 x 10mL) and was dried over sodium sulfate.

2A: (((naphthalene-1,5-diylbis(oxy))bis(ethane-2,1-diyl))bis(oxy))bis(ethane-2,1-diyl) bis(4-methylbenzenesulfonate)

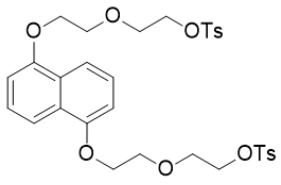

The diol substrate (1.0 g) was added to a flame-dried flask which was then dissolved in methylene chloride (15 mL). This solution was brought to 0 ºC and tosyl chloride (2.2 equiv) was added followed by triethylamine (2.5 equiv) and DMAP (0.1 equiv). This solution was allowed to warm to room temperature and its progress was monitored by TLC. Once completed 1M HCl was added and the layers were separated. Organic layer was washed with sat. sodium bicarb (1 x 10 mL), DI water (1 x 10mL), brine (1 x 10mL) and then dried over sodium sulfate and concentrated *in vacuo*. The resulting crude off white solid was recrystallized with hexanes to produce the desired bis-tosylated product.

3A: 4,4'-(((((naphthalene-1,5-diylbis(oxy))bis(ethane-2,1-diyl))bis(oxy))bis(ethane-2,1-diyl))bis(oxy))dibenzaldehyde

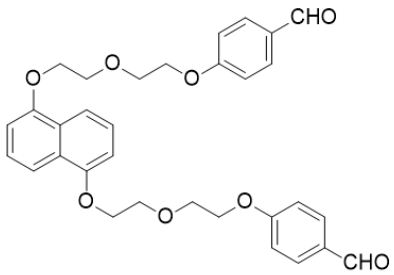

The starting material (500 mg) was added to a flame-dried flask which was then dissolved in dry DMF (10 mL). To this solution was added p-hydroxybenzaldehyde (2.5 equiv) and then potassium carbonate (5.5 equiv). The reaction was brought to 60 ºC and was stirred for 20 h. The crude reaction was vacuum filtered, rinsed with fresh cold DMF (2 x 10 mL) and then

dried over vacuum. The crude product was recrystallized in EtOH:methylene chloride (9:1) producing the desired dialdehyde.

6A: dimethyl 10,10'-(((1E,1'E)-((((((naphthalene-1,5-diylbis(oxy))bis(ethane-2,1-diyl))bis(oxy))bis(ethane-2,1-diyl))bis(oxy))bis(4,1-phenylene))bis(methaneylylidene))bis(azaneylylidene))bis(anthracene-9-carboxylate)

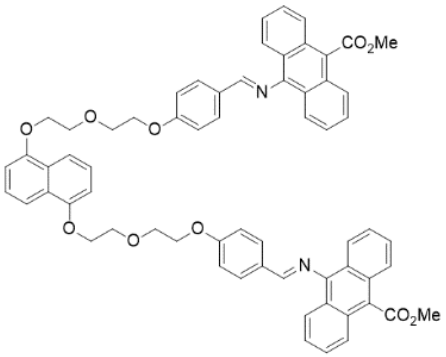

The starting material dialdehyde (341 mg) was added to a flam-dried flask and then dissolved in distilled methylene chloride (4 mL). 4 Å mol sieves were crushed to a powder via mortar pestle and then activated under high vacuum with heating and then cooled under high vacuum. The crushed mol sieves (1.28 g) were added to the reaction mixture which was then allowed to stir for 10 min. The anthraceneamine was then added along with pyrrolidine and the reaction was brought to 60 ºC. The progress of the reaction was monitored by TLC and once completed, was filtered and concentrated *in vacuo.* The crude rotaxane thread linker precursor was obtained in a 55% yield.

1E/2E: Diethyl 2,2'-(cyclohepta-2,4,6-trien-1-ylazanediyl)diacetate

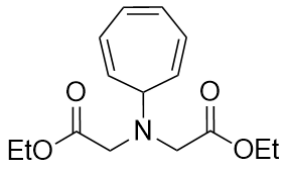

To a flame-dried round bottom was added NaH (634 mg) under inert atmosphere. The NaH was rinsed with THF (3 x 5mL) and then dried under vacuum. The NaH was suspended in THF (100 mL) a final time and then cooled to 0 ºC. The diethyl imidodiacetate (2.0 g) was added dropwise, allowed to warm to room temperate and then stirred for 30 min at 23 ºC. The tropylium BF_4 was then added in one addition and was stirred for 24 h at room

temperature. The reaction was quenched with 9mL DI water at 0 ºC and then extracted with 200 mL EtOAc. Organic layer was washed with water (1 x 50mL), brine (1 x 50 mL) and the dried over magnesium sulfate and the desired cycloheptatrienyl functionalized linker precursor was obtained in a 72% yield.

3E: Sodium 2,2'-(cyclohepta-2,4,6-trien-1-ylazanediyl)diacetate

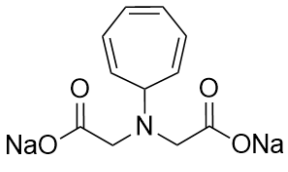

The substrate (100 mg) was dissolved in an acetone:EtOH mixture (2:3) and to this was added 6mL of 1.5M NaOH. After stirring for 15 mins, this reaction was then poured into another acetone:EtOH (1:3) mixture yielding a precipitate which was then filtered and washed with EtOH (3 x 10mL). The crude disodium salt was obtained and take forward in a 61% yield.

4.2 NMR Spectra for compounds synthesized in chapter 4

$CBPQT^{4+}$ Ring

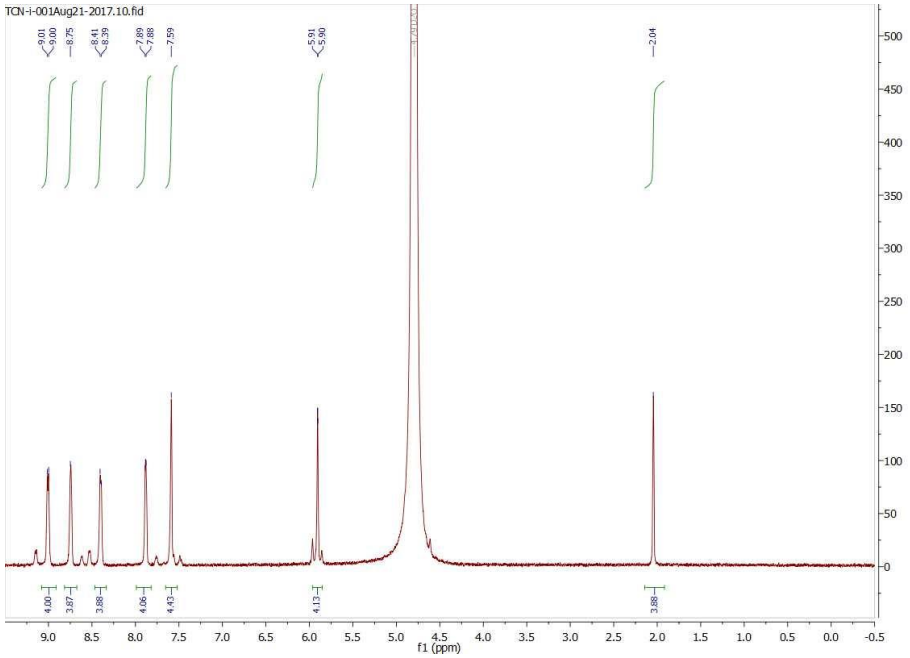

4A: Methyl 10-nitroanthracene-9-carboxylate

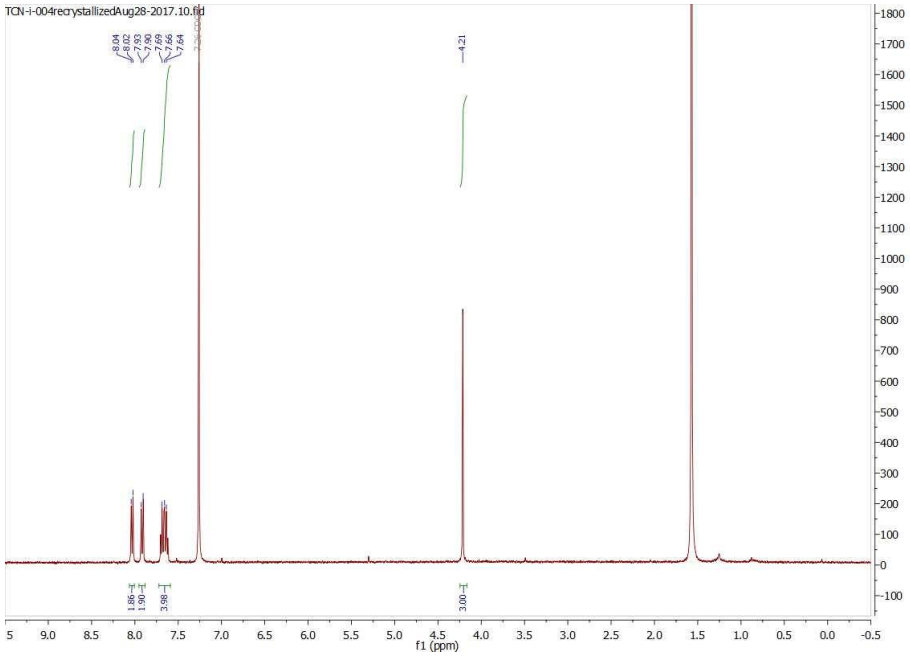

5A: Methyl 10-aminoanthracene-9-carboxylate

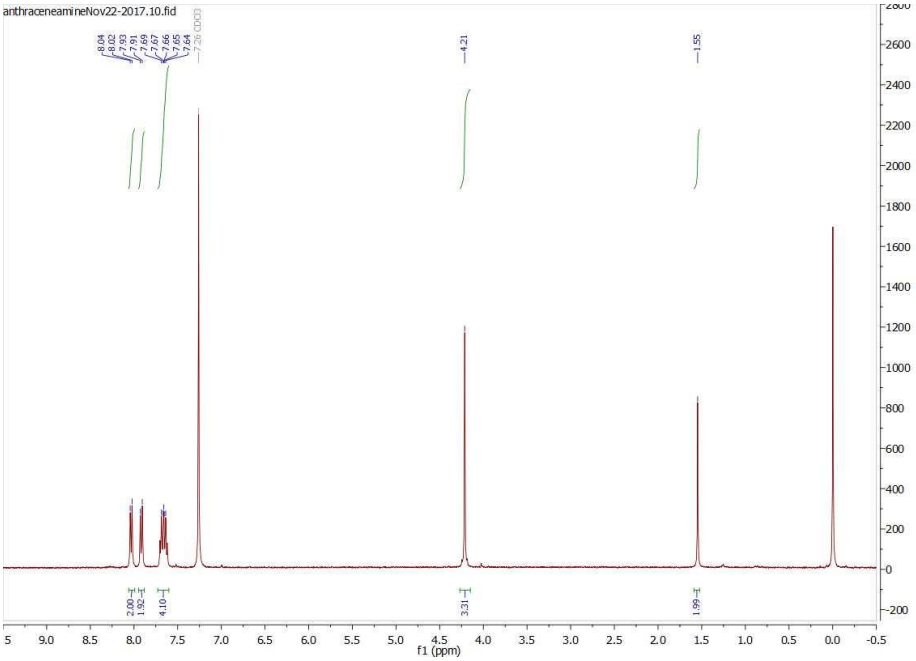

1A: 2,2'-(((naphthalene-1,5-diylbis(oxy))bis(ethane-2,1-diyl))bis(oxy))bis(ethan-1-ol)

NMR unavailable

2A: (((naphthalene-1,5-diylbis(oxy))bis(ethane-2,1-diyl))bis(oxy))bis(ethane-2,1-diyl) bis(4-methylbenzenesulfonate)

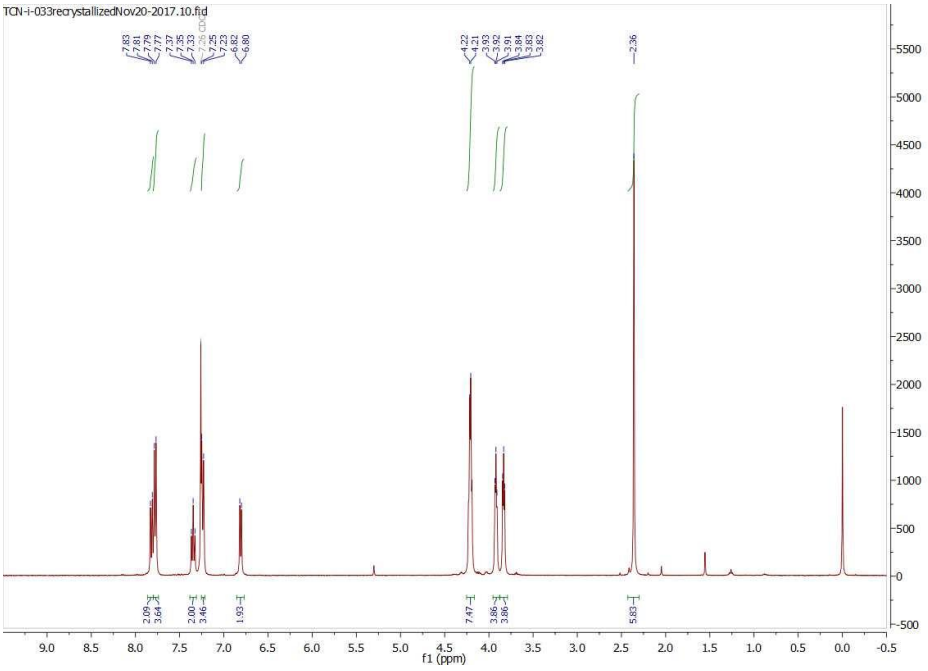

3A: 4,4'-(((((naphthalene-1,5-diylbis(oxy))bis(ethane-2,1-diyl))bis(oxy))bis(ethane-2,1-diyl))bis(oxy))dibenzaldehyde

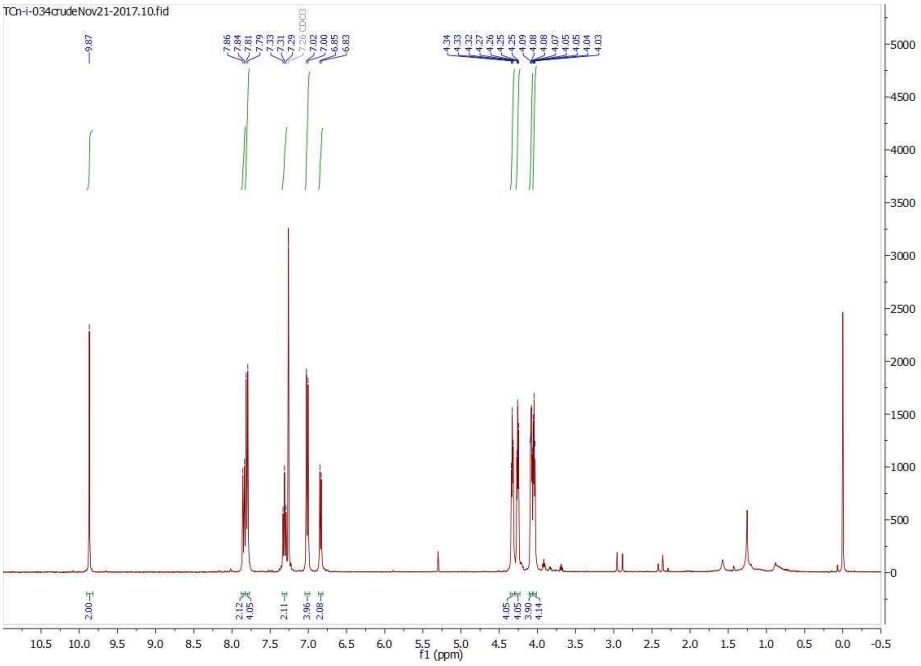

6A: dimethyl 10,10'-(((1E,1'E)-((((((naphthalene-1,5-diylbis(oxy))bis(ethane-2,1-diyl))bis(oxy))bis(ethane-2,1-diyl))bis(oxy))bis(4,1-phenylene))bis(methaneylylidene))bis(azaneylylidene))bis(anthracene-9-carboxylate)

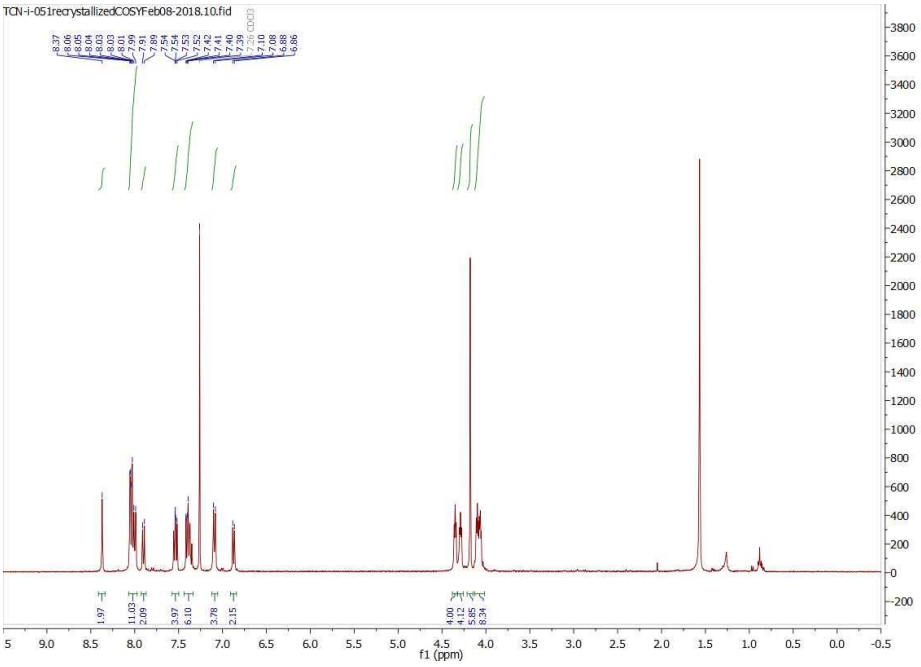

1E: Diethyl 2,2'-(cyclohepta-2,4,6-trien-1-ylazanediyl)diacetate

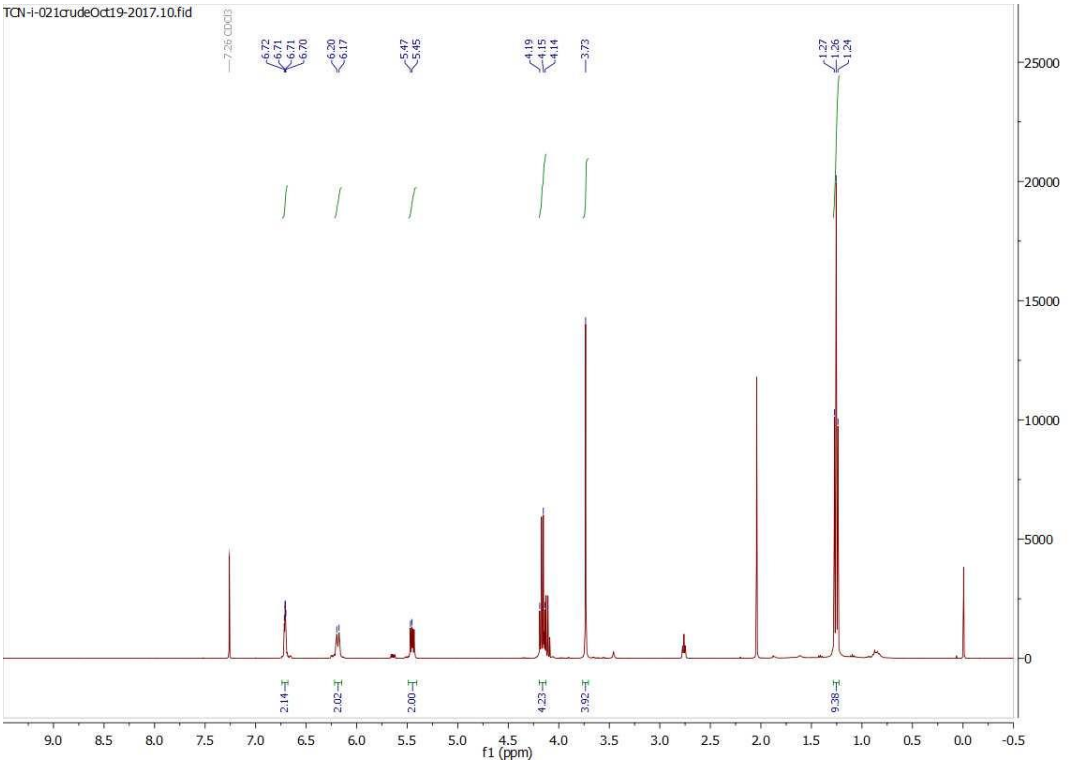

3E: Sodium 2,2'-(cyclohepta-2,4,6-trien-1-ylazanediyl)diacetate

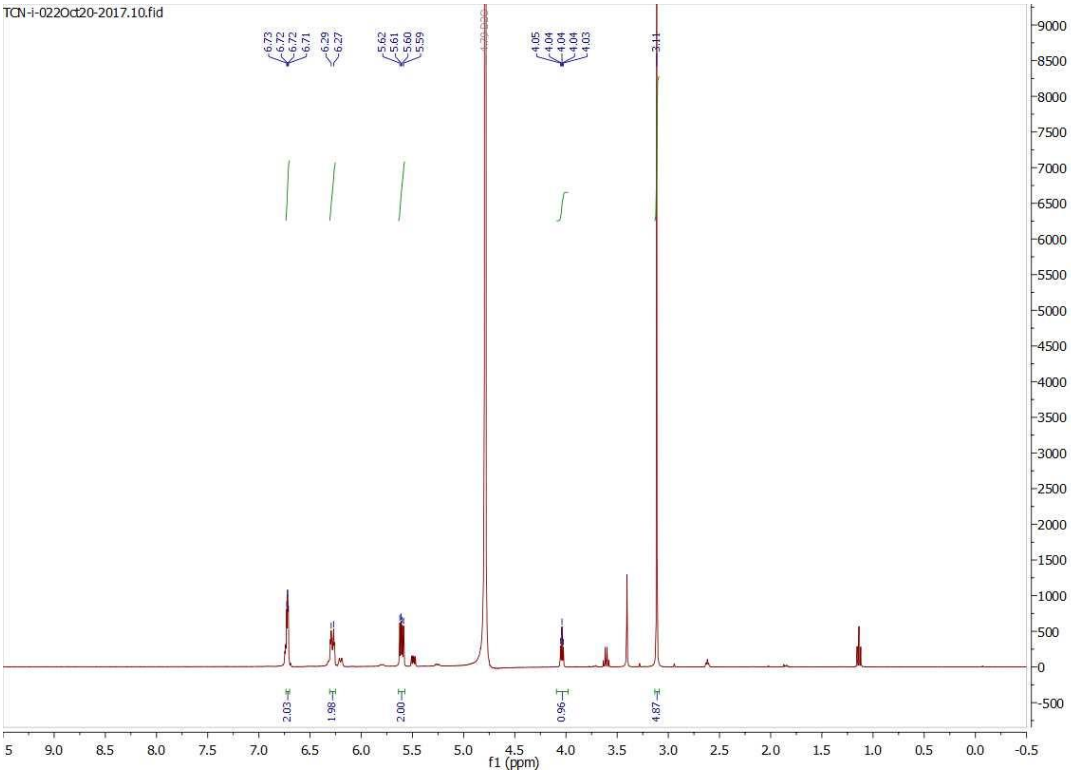

CHAPTER 5

O-NITROBENZYL CARBONATE AND O-NITROBENZYL ETHER MOF LINKERS

5.1 Synthesis of dibenzyl and terphenyl linker backbone

Once the linker backbone was decidedly a 4,4'-dibenzyldicarboxylic acid, a linker synthesis derived from p-terphenyl- 4,4'-dicarboxylic acid was proposed as well. This was because it was unclear at the time of the formation of this hypothesis as to whether the dibenzyl linker length would produce an adequate pore size. Initially, the two linkers were visualized to be functionalized with veratryl-derived o-nitrobenzyl carbonate linkages to act as the photolabile and gate moiety. At this time in the project development, my MOF was designed with zinc inorganic nodes as to take care to incorporate a biologically compatible metal into the framework. Zinc MOF pores exhibit cubical pore geometry which would produce a functionalized pore theoretically with a o-nitrobenzyl carbonate gate existing close to each pore face. A simplified depiction is seen in Figure 15.

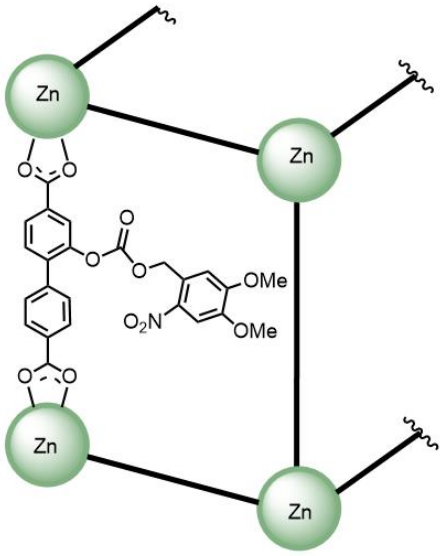

Figure 15. Depiction of zinc-based MOF pore constructed with proposed carbonate ligated o-nitrobenzyl photolyzable group.

It is important to note that three-dimensionally, it is unreasonable to believe one of the o-nitrobenzyl gates will act as a true "door" and remain oriented within the plane of the pore surface. It is more reasonable to theorize the gate moiety orienting slightly

inward toward the pore center in order to optimize electronic repulsion effects of the o-nitrobenzyl carbonate and the di or terphenyl linker backbone. Nevertheless, it is still reasonable to believe that the gate moieties incorporated into the MOF still have the ability to mechanically trap guest molecules within the pores they are functionalized onto. Therefore, the synthesis of the dibenzyl and terphenyl backbone linker was proposed, complete with a hydroxyl functionality. Concomitantly, the o-nitrobenzyl derivative was synthesized alongside these linker backbones. With the backbone decorated with a hydroxyl handle, the o-nitrobenzyl gate would then be affixed to the backbone initially via carbonate linkage, however later on this would optimized to an ether linkage.

The di-benzyl hydroxyl backbone synthesis began with p-bromobenzaldehyde dimethyl acetal which was converted to (4-formylphenyl)boronic acid in a lithium halogen exchange with subsequent addition into triisopropyl borate in an 70% yield. The phenyl boronic acid was then coupled together with one addition of p-bromobenzaldehyde dimethyl acetal in a Suzuki palladium cross coupling reaction in a 78% yield to produce 4,4'-dibenzyldicarbalehyde. This dialdehyde was then oxidized to the methyl ester in Yamada oxidation conditions in the presence of MeOH with KOH and I_2. The above synthesis was utilized for a short time until dimethyl biphenyl-4,4'-dicarboxylate was obtained commercially. With the linker backbone in hand, it was time to functionalize one of the benzene two positions with a hydroxyl group to allow for the installation of the o-nitrobenzyl ester. To begin the second part of this synthesis, dimethyl biphenyl-4,4'-dicarboxylate was nitrated at the two position in simple HNO_3/H_2SO_4 conditions in quantitative yields. Careful control of stoichiometry of the HNO_3 is

essential to the formation of the mono-nitrated product. The nitro group was then initially reduced to the amine via reductive $SnCl_2$ conditions in a 56% yield, however this reaction was later optimized to pressurized H_2 Pd/C conditions with improved yields of up to 87% conversion. To accomplish the installation of the hydroxyl group, the nitro derivative of dimethyl biphenyl-4,4'-dicarboxylate was taken on in Sandmeyer type chemistry, obtaining the phenol group through a phenyl diazo in an 80% yield. With the appropriately functionalized dibenzyl linker backbone, attempts were made at the synthesis of the terphenyl derivative.

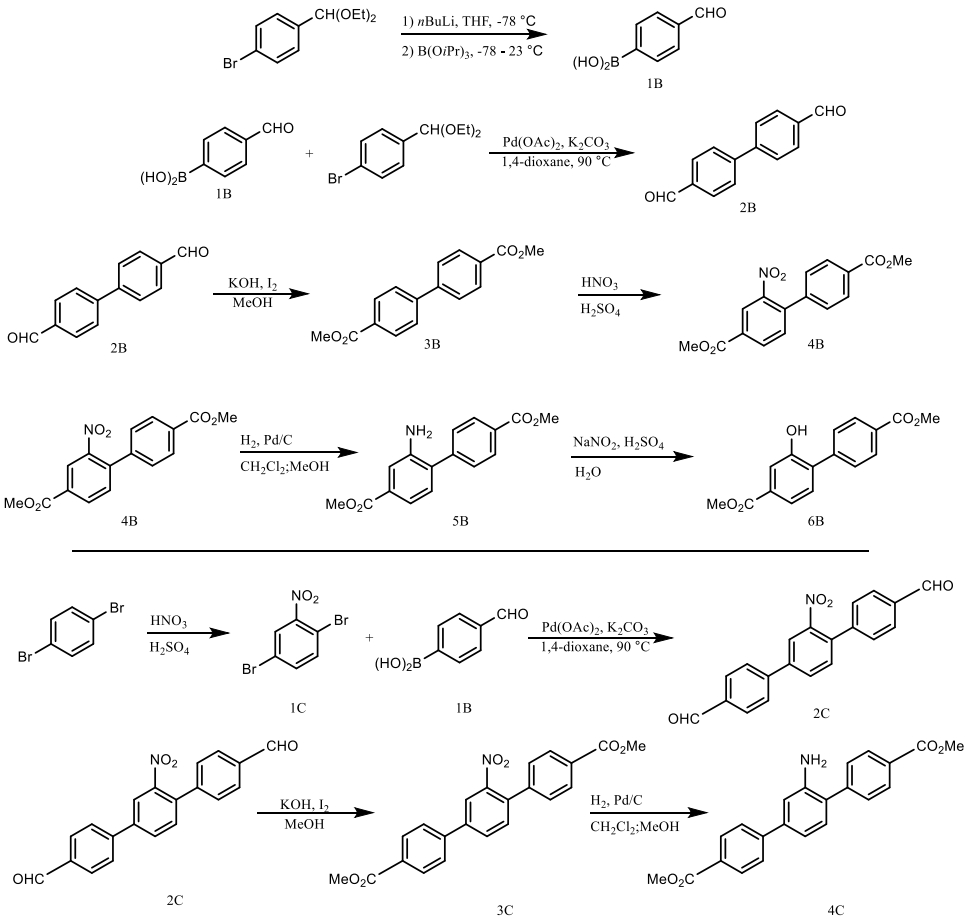

Scheme 2. Full syntheses for both the diphenyl linker backbone functionalized with a hydroxyl group, and the terphenyl linker backbone which was synthesized to the amine functionality. If future work is to be done with the terphenyl derived linker, the syntheses of said linker would be simply accomplished via chemistry developed for the diphenyl linker.

To synthesize the terphenyl linker, it was proposed to utilize the already synthesized (4-formylphenyl)boronic acid in a Suzuki coupling with 1,4-dibromo-2-nitrobenzene in order to use the nitro group as a handle to install a hydroxyl functionality later in the synthesis. 1,4-dibromo-2-nitrobenzene was synthesized in a nitration reaction with 1,4-dibromobenzene readily in quantitative yields. Suzuki cross coupling of the terphenyl linker precursor was accomplished with $Pd(OAc)_2$, the produced 1,4-dibromo-2-nitrobenzene and two equivalents of (4-formylphenyl)boronic acid. Much like the previous synthesis, the nitro derivative of the terphenyl linker was reduced to the amine via reductive $SnCl_2$ conditions. However, following conversion to the amine, concentration fell heavily on the utilization of the diphenyl linker backbone and so the next immediate steps were taken to synthesize the photolyzable group. Full syntheses for both the dibenzyl and terphenyl linker amine are presented in figure Scheme 2.

5.2 Synthesis of o-nitrobenzyl carbonate and optimization to ether linkage

The synthesis of the o-nitrobenzyl carbonate group began with nitration of veratraldehyde ortho to the aldehyde functionality in a quantitative conversion. Reduction of the aldehyde to the benzyl alcohol was accomplished via $NaBH_4$ reduction in a 98% yield. With the desired benzyl alcohol and dibenzyl phenol in hand, the carbonate formation was accomplished in a 69% yield via coupling of the two alcohols with bis(trichloromethyl) carbonate (BTC) as a method of generating triphosgene *in situ*. The full synthesis of the o-NB alcohol, o-NB chloride, the BTC coupling reaction and the o-NB ether formation can be seen in Scheme 2. With the desired carbonate in hand the

saponification of the methyl esters was attempted to form the dicarboxylic acid thus forming the MOF linker.

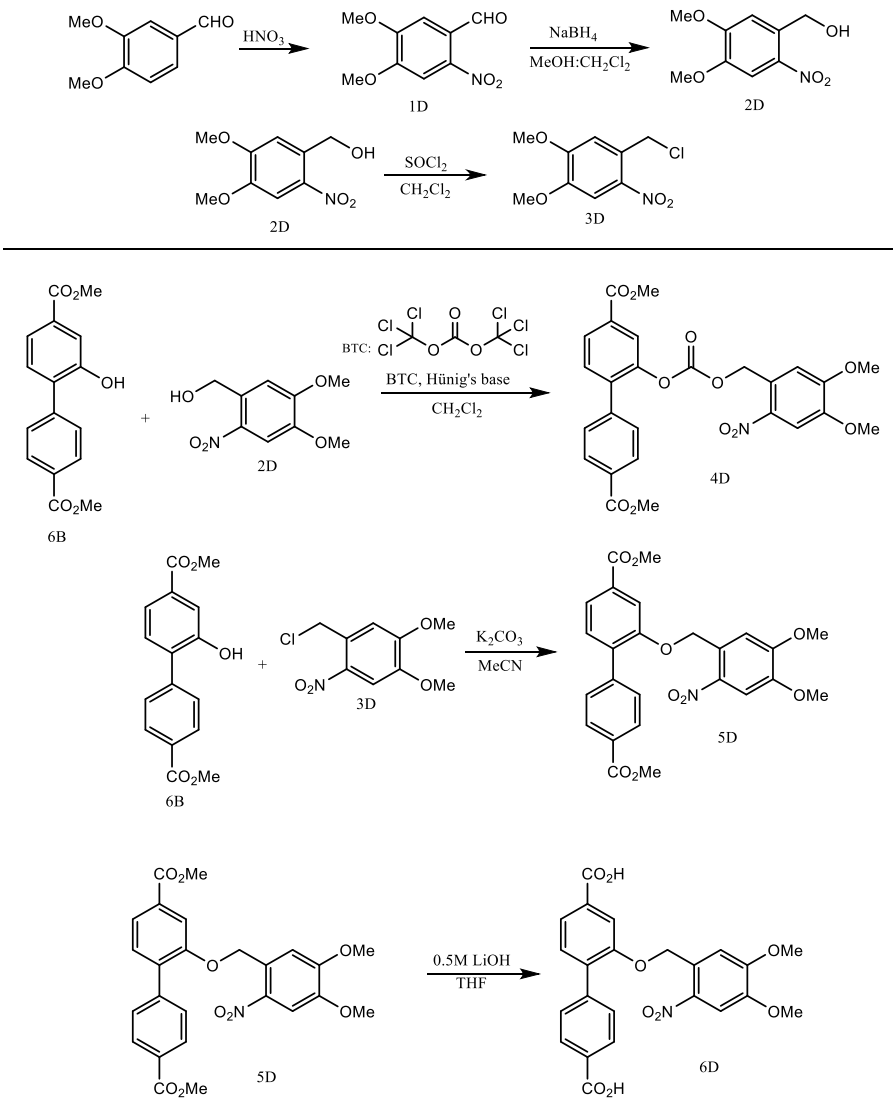

Scheme 3. Synthesis for the o-nitrobenzylalcohol and rection scheme for the coupling of the linker backbone and the o-nitrobenzyl alcohol to form the desired carbonate linker diester precursor.

As with the attempts made with the 1,3,5-cycloheptatrienyl functionalized MOF linker, the saponification of this linker precursor also proved difficult. I was unable to obtain the diacid from the re-acidification subsequent to the base catalyzed

saponification, observing only the deprotection of the phenolic oxygen. Because of this difficulty, a simple and logical shift away from the carbonate connected o-nitrobenzyl photolabile group, to an ether connected o-nitrobenzyl group. Changing the synthesis to produce the o-NB ether was straight forward and only required an additional reaction to be added to the o-nitrobenzyl synthesis. Following the $NaBH_4$ reduction in this synthesis, compound 2D was then submitted to thionyl chlorination reaction conditions, where the benzyl chloride 3D was obtained in a 90% yield. To obtain the ether linkage, compound 3D and diphenol linker backbone 6B were then reacted in soft base SN2 conditions to successfully reveal MOF linker precursor compound 5D in a 97% yield.

As with all other attempts to generate the diacid MOF linker, this saponification was challenging, yet produced much more promising results initially. The first attempts were made with aq. $LiOH/H_2O_2$ in THF as the solvent to aid in the dissolution of the starting material. The very first reaction, complete deprotection of the phenolic oxygen was all that was observed. However, optimization through the tuning of reaction conditions did lead to desired product formation. It was ultimately found that at 25 ºC and for 16 hr, in molarities around 0.001M, in the presence of 0.5M LiOH and THF, this saponification can generate the desired diacid MOF linker 6D in modest yields (75-80% yield).

There are several crucial particulars needed to be cared for to allow this reaction to be successful. Firstly, the reaction should run no longer than 16 hours, and should be heavily monitored by TLC. On some iterations of this reaction, running longer than 16 hours will produce significant amounts of deprotected product, which make purification of this material very difficult. Secondly, the reaction must be run in dark conditions to

avoid the photolyzed deprotected of the o-nitrobenzyl group. When dissolved, it has been observed that this deprotection is more facile than as opposed to when the material is in a solid state. Following complete conversion to the desired diacid product, the THF must then be removed from the aqueous LiOH via roto evaporation. Thirdly, during the dark reacidification of the resulting basic aqueous solution of the dianion, it is crucial to begin and maintain the slow, dropwise addition of the 1M HCl at 0 ºC. In addition to this, the pH of the reacidification must not reach below a pH of 3. A pH of this strength is adequate to re-protonate the dicarboxylates, however further acidification will produce the undesired deprotected linker backbone. Optimizing this reaction in these ways allows for the successful synthesis of the full gate functionalized MOF linker (spectra 6D). With the full linker in hand, it was then time to begin the optimization of the desired MOF material.

A noteworthy mention here is that at this point in the project, no MOF synthesis had been attempted before, apart from one microwave synthesis utilizing the failed sodium dianion salt of the 1,3,5-cycloheptatrienyl linker. In addition to this, as a chemist, I was experimentally unfamiliar with MOF syntheses and the parameters to modulate to attempt a MOF synthesis optimization. Then, following the synthesis, materials characterization was also an unfamiliar area. A dramatic shift in focus from the organic synthesis of the MOF linker, to the materials synthesis of a functional MOF material would prove quite challenging, yet ultimately rewarding. Moving forward, much learning through experience would be made, and importantly, aid would be given providing the research a much clearer direction.

5.1 Detailed procedures for reactions within chapter 5

1B: (4-formylphenyl)boronic acid

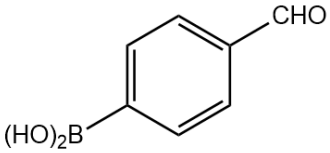

To a flame-dried round bottom flask was added the substrate (3.5 mL) and THF (150 mL) and this mixture was then cooled to -78 ºC. After cooling, *n*BuLi was added dropwise and this solution was stirred for 60 min at -78 ºC. B(*i*OPr)$_3$ was then added dropwise at -78 ºC and then further reacted for 12h, allowing the reaction to warm up to room temperature. The reaction was quenched with 3M HCl (15 mL) and then stirred for 3h to hydrolyze the borate. The organic layer was allowed to partition, and the aqueous layer was extracted with EtOAc (3 x 40mL). Combined organic layers were then washed with DI H_2O (2 x 20 mL), brine (2 x 20 mL) and then dried over magnesium sulfate affording the desired boronic acid in a 65% yield.

2B: [1,1'-biphenyl]-4,4'-dicarbaldehyde

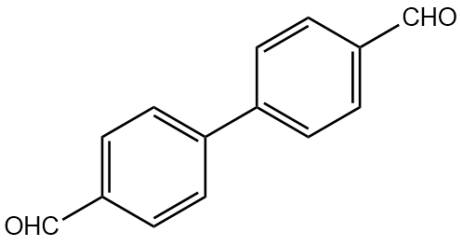

Boronic acid (100 mg) and aryl bromide (1 equiv) was added to flame-dried round bottom which was then dissolved in distilled 1,4-dioxane (6 mL). Under inert atmosphere this solution was degassed via argon balloon for 30 min. Pd(OAc)$_2$ was then added to the reaction followed by potassium carbonate and this reaction was stirred at reflux until completion was confirmed by TLC. After completion, crude reaction was diluted with THF and then passed through a celite filter. Crude product was purified via column chromatography (10% EtOAc in Hex) and the dialdehyde was obtained in a 55% yield.

3B: dimethyl [1,1'-biphenyl]-4,4'-dicarboxylate

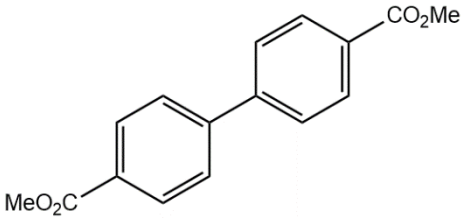

Dialdehyde substrate (100 mg) was dissolved in MeOH (8 mL) while I_2 (460 mg) and KOH (201 mg) were both dissolved separately in 2mL MeOH each. The substrate solution was cooled to 0 ºC and the KOH solution was added to the substrate first at 0 ºC which was then followed quickly by the I_2 solution. The reaction was monitored by TLC and once completed, MeOH was removed *in vacuo*. The crude product was redissolved in methylene chloride which was then washed with water (3 x 5mL), sodium bisulfite (2 x 5 mL) and brine (2 x 5mL). The crude product was concentrated *in vacuo* and then purified via column chromatography (20% EtOAc in Hex) and the dimethyl ester was obtained in a quantitative yield.

4B: dimethyl 2-nitro-[1,1'-biphenyl]-4,4'-dicarboxylate

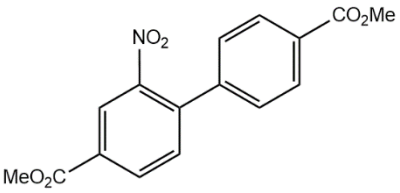

Diester was suspended in H_2SO_4 and allowed to stir for 10 min to fully dissolve. This solution was then cooled to 0 ºC before adding a solution of nitric acid (1 equiv) in H_2SO_4 slowly dropwise. The then reaction was allowed to warm to room temperature and stir for 1h at 23 ºC. Pouring the finished crude reaction into an ice slurry precipitated the desired crude nitro compound, which was then filtered, rinsed with water (3 x 20 mL) and immediately recrystallized in EtOH affording the desired nitro derivative in a quantitative yield.

5B: dimethyl 2-amino-[1,1'-biphenyl]-4,4'-dicarboxylate

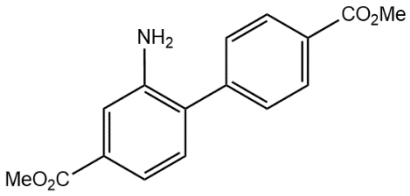

To a flame-dried flask under N_2 gas was added the Pd/C powder (400 mg). This flask was then sealed and then evacuated with vacuum and then resubmitted to N_2 atmosphere (x3). Methylene chloride (60 mL) was then added to the powder under inert atmosphere taking care to rinse the sides of the flask to bring he Pd/C powder into the solution. Once all of the Pd/C powder was under solvent, MeOH (60 mL) was added. The substrate (3.4 g) was dissolved in a small portion of methylene chloride (10 mL) and then added to the Pd/C mixture as well and was stirred to distribute. This mixture was again evacuated and flushed back with nitrogen (x3). On the final evacuation with vacuum, a hydrogen balloon was inserted instead of the last nitrogen backfill. The reaction was monitored by TLC until completed. Once reaction was complete the mixture was poured and filtered over celite taking care to not allow to bed of celite to dry. The crude reaction was the concentrated *in vacuo* and then recrystallized with EtOH affording the desired amine in an 87% yield.

6B: dimethyl 2-hydroxy-[1,1'-biphenyl]-4,4'-dicarboxylate

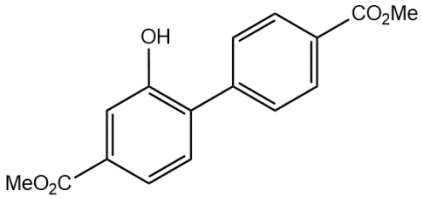

The amine substrate (1.25 g) was suspended in an aqueous solution of H_2SO_4 (22.5 mL in 120 mL H_20). This solution was chilled to 0 ºC and stirred for 10 mins to allow to dissolution of substrate. At 0 ºC a solution of sodium sulfite (239 mg) in water (40 mL) was added dropwise with vigorous stirring. After full addition, the ice bath was removed, and the reaction was allowed to warm to room temperature and was stirred there for 30 mins. The reaction was then placed in a hot oil bath that was preheated to 90

ºC which was then set to 110 ºC. Once the reaction reached 110 ºC, it was stirred vigorously at this temperature for 5 mins and then cooled in an ice bath. Once cooled the resulting solid was filtered, washed with water (3 x 50 mL) and could be recrystallized in EtOH or purified via column chromatography (3% MeOH in methylene chloride). The desired phenol was obtained in an 80% isolated yield.

1C: 1,4-dibromo-2-nitrobenzene

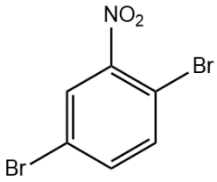

1,4-dibromobenzene (5.9 g) was dissolved in 15 mL of methylene chloride to which was added a solution of nitric acid (1.77 mL) and sulfuric acid (3.75 mL). This nitric acid solution was added dropwise to stirring solution of substrate until strong blue color turned to dark yellow. Reaction was quenched with 25 % (wt/v) NaOH (2 mL), extracted with methylene chloride (3 x 50 mL) and the organic layer was washed with water (2 x 20 mL) brine (2 x 20mL) and then dried over sodium sulfate. Crude nitro compounds was then purified via recrystallization with EtOH and which produced the pure nitro compound in a quantitative yield.

2C: 2'-nitro-[1,1':4',1"-terphenyl]-4,4"-dicarbaldehyde

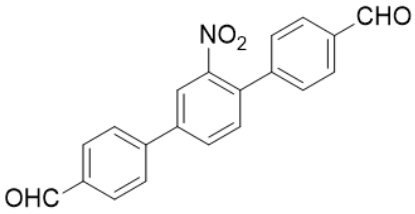

Boronic acid (2 equiv) and aryl dibromide (1 equiv) were added to flame-dried round bottom which was then dissolved in distilled 1,4-dioxane (6 mL). Under inert atmosphere this solution was degassed via argon balloon for 30 min. $Pd(OAc)_2$ was then added to the reaction followed by potassium carbonate and this reaction was stirred at reflux until completion was confirmed by TLC. After completion, crude reaction was diluted with THF and then passed through a celite filter. Crude product was purified via

column chromatography (10% EtOAc in Hex) and the desired dialdehyde was afforded in a 52% yield.

3C: dimethyl 2'-nitro-[1,1':4',1''-terphenyl]-4,4''-dicarboxylate

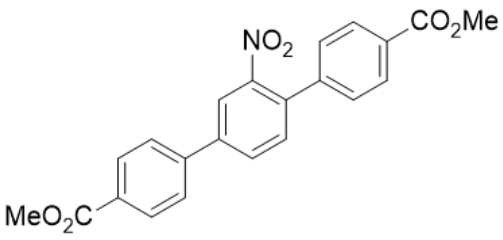

Dialdehyde substrate (100 mg) was dissolved in MeOH (8 mL) while I_2 (460 mg) and KOH (201 mg) were both dissolved separately in 2mL MeOH each. The substrate solution was cooled to 0 ºC and the KOH solution was added to the substrate first at 0 ºC which was then followed quickly by the I_2 solution. The reaction was monitored by TLC and once completed, MeOH was removed *in vacuo*. The crude product was redissolved in methylene chloride which was then washed with water (3 x 5mL), sodium bisulfite (2 x 5 mL) and brine (2 x 5mL). The crude product was concentrated *in vacuo* and then purified via column chromatography (20% EtOAc in Hex) affording the desired dimethyl ester in a quantitative yield.

4C: dimethyl 2'-amino-[1,1':4',1''-terphenyl]-4,4''-dicarboxylate

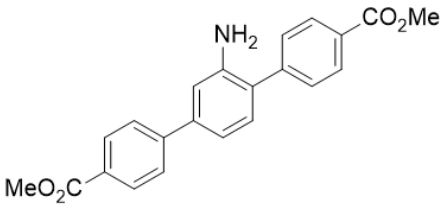

To a flame-dried flask under N_2 gas was added the Pd/C powder (400 mg). This flask was then sealed and then evacuated with vacuum and then resubmitted to N_2 atmosphere (x3). Methylene chloride (60 mL) was then added to the powder under inert atmosphere taking care to rinse the sides of the flask to bring he Pd/C powder into the solution. Once all of the Pd/C powder was under solvent, MeOH (60 mL) was added. The substrate (3.4 g) was dissolved in a small portion of methylene chloride (10 mL) and then added to the Pd/C mixture as well and was stirred to distribute. This

mixture was again evacuated and flushed back with nitrogen (x3). On the final evacuation with vacuum, a hydrogen balloon was inserted instead of the last nitrogen backfill. The reaction was monitored by TLC until completed. Once reaction was complete the mixture was poured and filtered over celite taking care to not allow to bed of celite to dry. The crude reaction was the concentrated *in vacuo* and then recrystallized with EtOH, affording the desired amine in a 84% yield.

1D: 4,5-dimethoxy-2-nitrobenzaldehyde

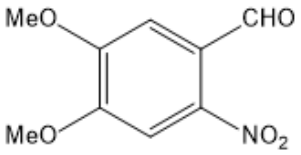

Veratraldehyde (4.0 g) was suspended in H_2SO_4 (20 mL) and allowed to stir for 10 min to fully dissolve. This solution was then cooled to 0 ºC before adding a solution of nitric acid (1 equiv) in H_2SO_4 (5 mL) slowly dropwise. The then reaction was allowed to warm to room temperature and stir for 1h at 23 ºC. Pouring the finished crude reaction into an ice slurry precipitated the desired crude nitro compound, which was then filtered, rinsed with water (3 x 20 mL) and immediately recrystallized in EtOH affording the desired nitroaldehyde in a quantitative yield.

2D: (4,5-dimethoxy-2-nitrophenyl)methanol

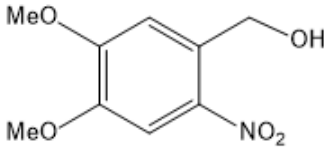

substrate (1.0 g) was added to a flame-dried flask and dissolved in 48 mL of a solution of MeOH:methylene chloride (3:1). This mixture was then cooled to 0 ºC and the $NaBH_4$ (358 mg) was added in 3 portions. Reaction was allowed to warm to room temperature and was monitored by TLC and quenched with 20 mL of water upon completion. MeOH was removed *in vacuo* and then the crude product was diluted with 20 mL methylene chloride. Organic layer was washed with water (3 x 20 mL) and then

brine (2 x 20 mL) and then dried over sodium sulfate. The crude product was purified via column chromatography (50% EtOAc in Hex) and the desired benzylalcohol was produced in a 98% yield.

3D: 1-(chloromethyl)-4,5-dimethoxy-2-nitrobenzene

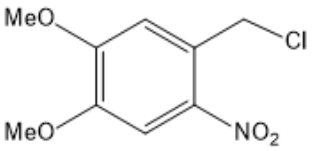

benzyl alcohol substrate (200 mg) was added to a flame-dried flask and then dissolved in methylene chloride (10 mL). This solution was cooled to 0 ºC and to it was added triethylamine (2 drops) and thionyl chloride (146 µL). Reaction was allowed to warm to room temperature and then stirred overnight. The reaction was quenched with water (5 mL) and the aqueous layer was extracted with methylene chloride (3 x 10 mL) and the combined organic layers were washed with water (3 x 10 mL), brine (3 x 10 mL) and then dried over sodium sulfate. The crude benzyl chloride was then purified via column chromatography (20% EtOAc in Hex) which was obtained in a 90% isolated yield.

4D: dimethyl 2-((((4,5-dimethoxy-2-nitrobenzyl)oxy)carbonyl)oxy)-[1,1'-biphenyl]-4,4'-dicarboxylate

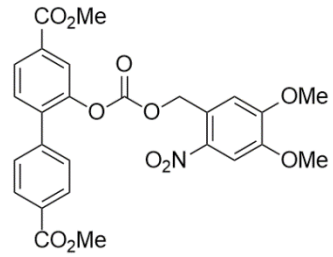

To a flame-dried round bottom flask was added bis(trichloromethyl)carbonate (19 mg) and distilled methylene chloride (2 mL). This solution was cooled to 0 ºC and then a 2mL solution of dimethyl 2-hydroxy-[1,1'-biphenyl]-4,4'-dicarboxylate (50 mg) in methylene chloride was added to the BTC solution dropwise over 30 min. The reaction was allowed to stir at 0 ºC for 30 mins then a solution of (4,5-dimethoxy-2-nitrophenyl)methanol (37 mg) in 500 µL of methylene chloride and 33 µL of Hunigs base were added quickly. This reaction was allowed to

warm up to room temperature and stir for 60 mins. After completion was confirmed by TLC, the solvent was removed *in vacuo* and then taken up in EtOAc (10 mL). The resulting crude reaction was washed with 5% HCl (1 x 5mL), sat. sodium bicarbonate (1 x 5mL), water (1 x 5mL), brine (1 x 5 mL) and then dried over magnesium sulfate. The resulting solid was kept in the dark and rinsed with diethyl ether and dried *in vacuo* and taken on crude in a 93% yield to the saponification step.

5D: dimethyl 2-((4,5-dimethoxy-2-nitrobenzyl)oxy)-[1,1'-biphenyl]-4,4'-dicarboxylate

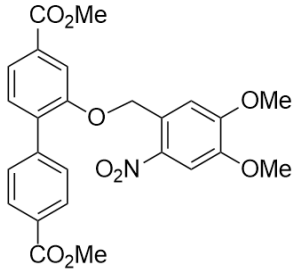

The substrate phenol (1 equiv) was dissolved in distilled MeCN which was warmed to 70 ºC and allowed to dissolve over 10 minutes. Potassium carbonate (4 equiv) was then added to the warmed mixture followed by 1-(chloromethyl)-4,5-dimethoxy-2-nitrobenzene (1 equiv). This reaction was allowed to stir overnight, and the resulting precipitate was dissolved in chloroform until no solid product remained. The solution was vacuum filtered to remove potassium carbonate, concentrated *in vacuo,* and the crude o-nitrobenzyl ether produced in a 97% yield, was taken on to the saponification step.

6D: 2-((4,5-dimethoxy-2-nitrobenzyl)oxy)-[1,1'-biphenyl]-4,4'-dicarboxylic acid

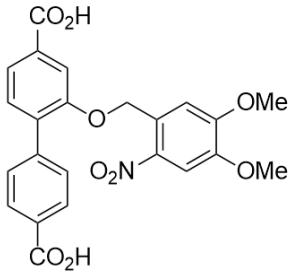

The substrate diester (1.0g) is suspended in THF (20 mL) and this solution is very gently heated with a heat gun to encourage dissolution of starting material in THF. Once dissolved, this solution was allowed to cool down to room temperature and then put into dark condition by covering the round bottom flask with aluminum foil. 50 mL of 0.5M LiOH solution was added to starting material and then allowed to stir

overnight. Longer stirring times will result in deprotecting of benzyl ether. Crude reaction was then concentrated *in vacuo* to remove THF solvent and then cooled to 0 ºC for 5 mins. Under dark conditions, the saponified lithium dianion was re-acidified with 10% (v/v) HCl dropwise until a pH of ~3.5 was reached. Precipitated diacid linker was immediately filtered and rinsed with water (3 x 50 mL) and then placed in a flask containing 50 mL MeOH and this was stirred for 15 mins. Desired MOF linker was afforded in a 80% yield, filtered, and dried overnight under high vacuum and stored at 5 ºC in the dark.

5.2 NMR Spectra for all compounds synthesized in chapter 5

1B: (4-formylphenyl)boronic acid

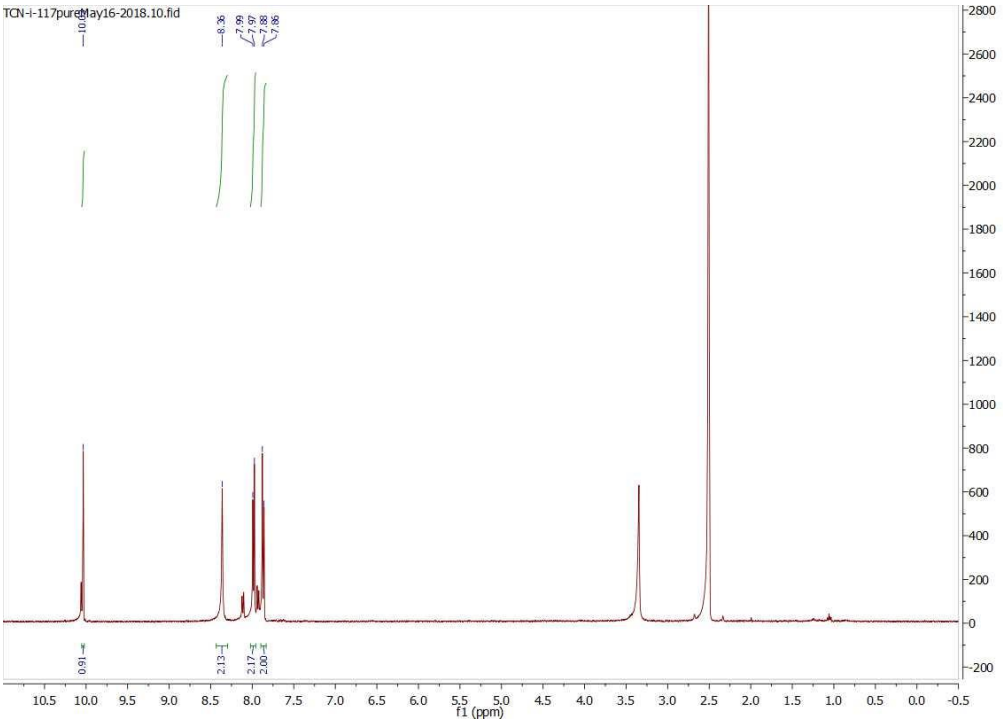

2B: [1,1'-biphenyl]-4,4'-dicarbaldehyde

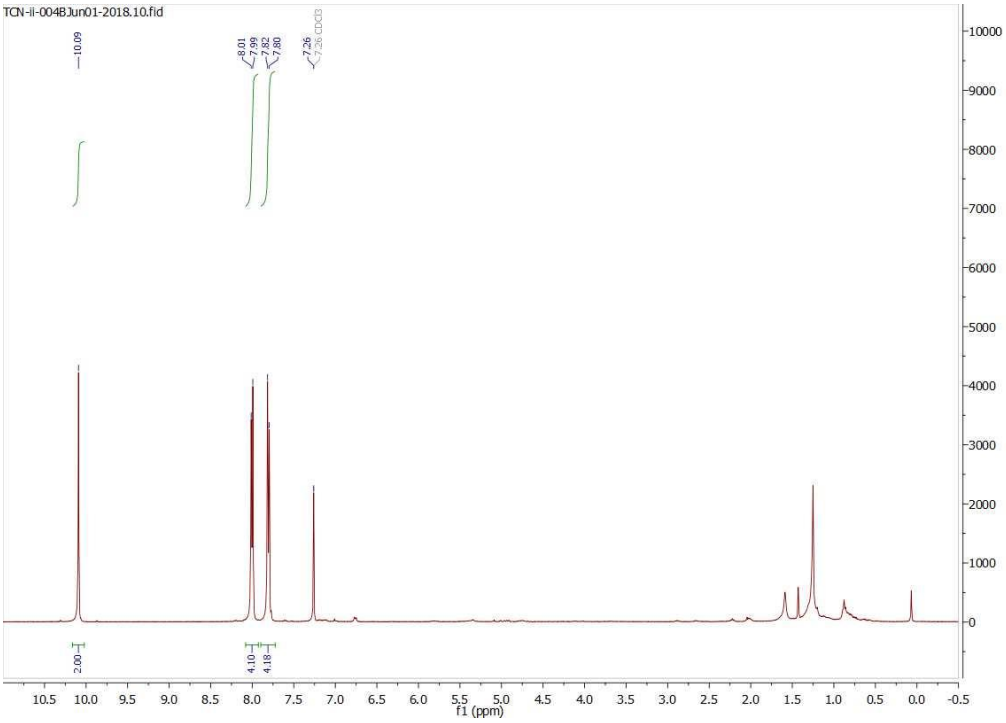

3B: dimethyl [1,1'-biphenyl]-4,4'-dicarboxylate

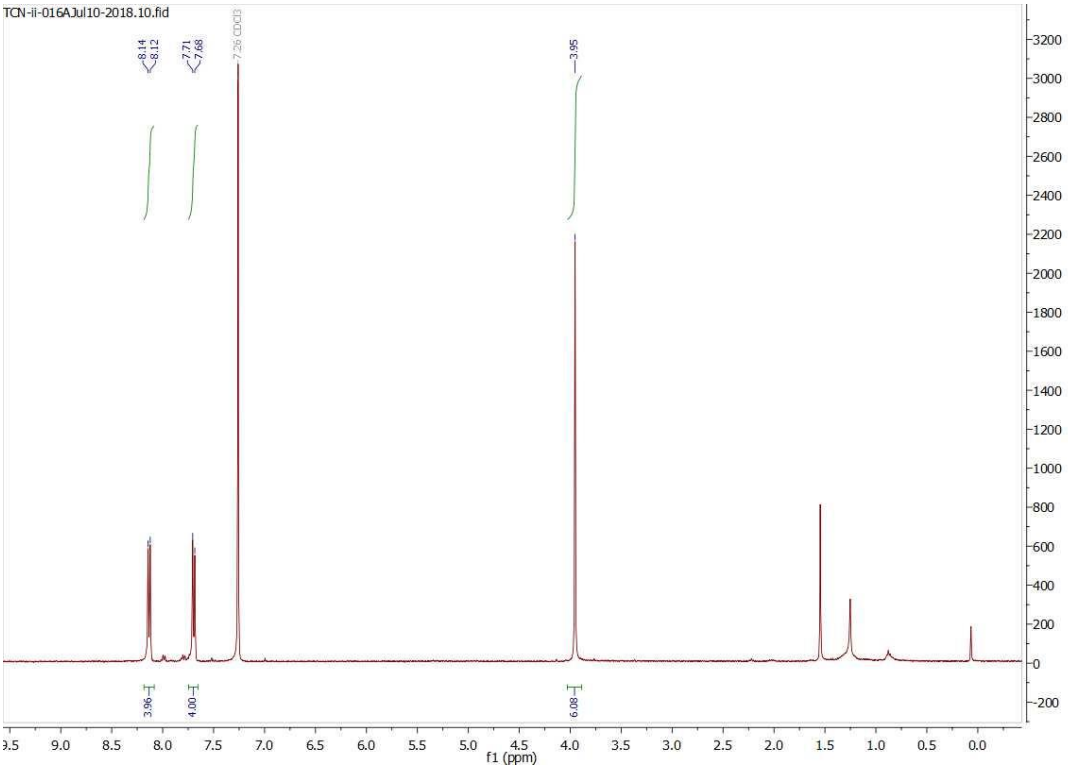

4B: dimethyl 2-nitro-[1,1'-biphenyl]-4,4'-dicarboxylate

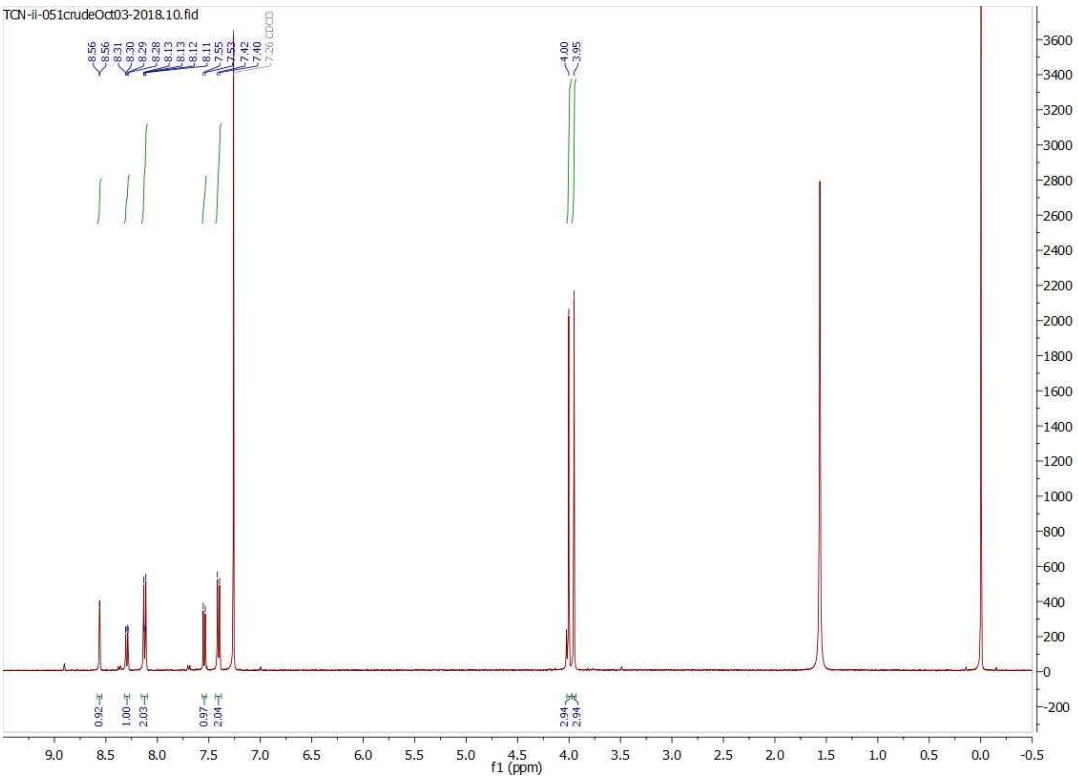

5B: dimethyl 2-amino-[1,1'-biphenyl]-4,4'-dicarboxylate

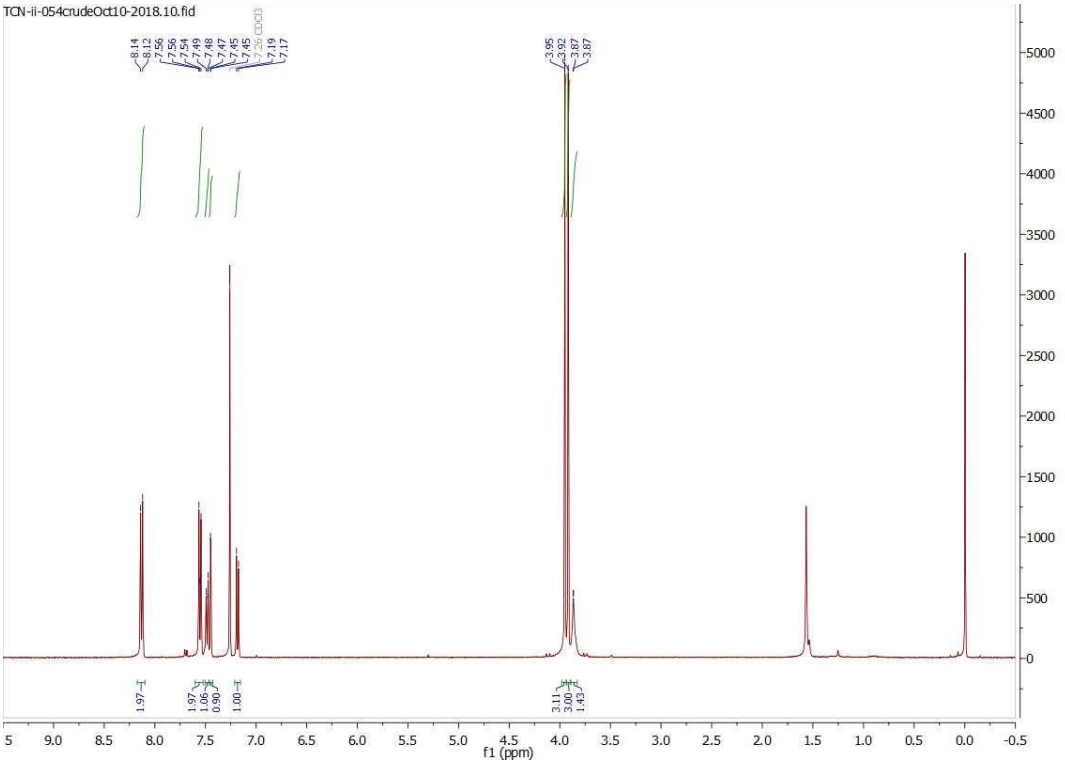

6B: dimethyl 2-hydroxy-[1,1'-biphenyl]-4,4'-dicarboxylate

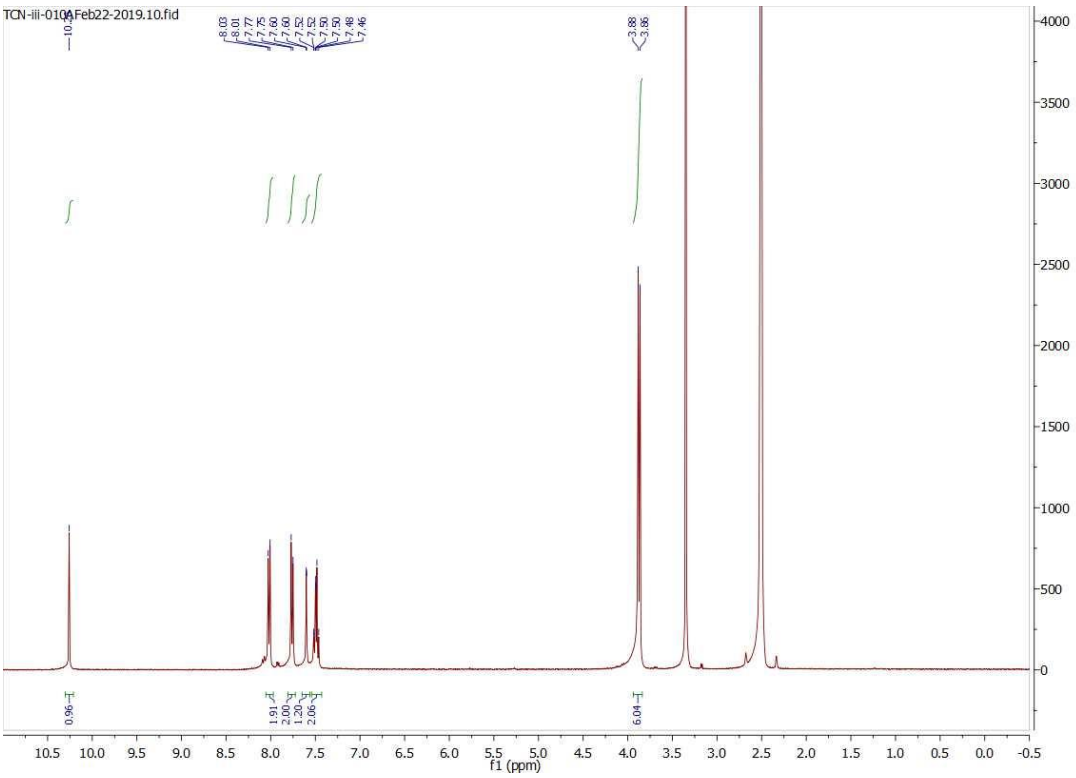

1C: 1,4-dibromo-2-nitrobenzene

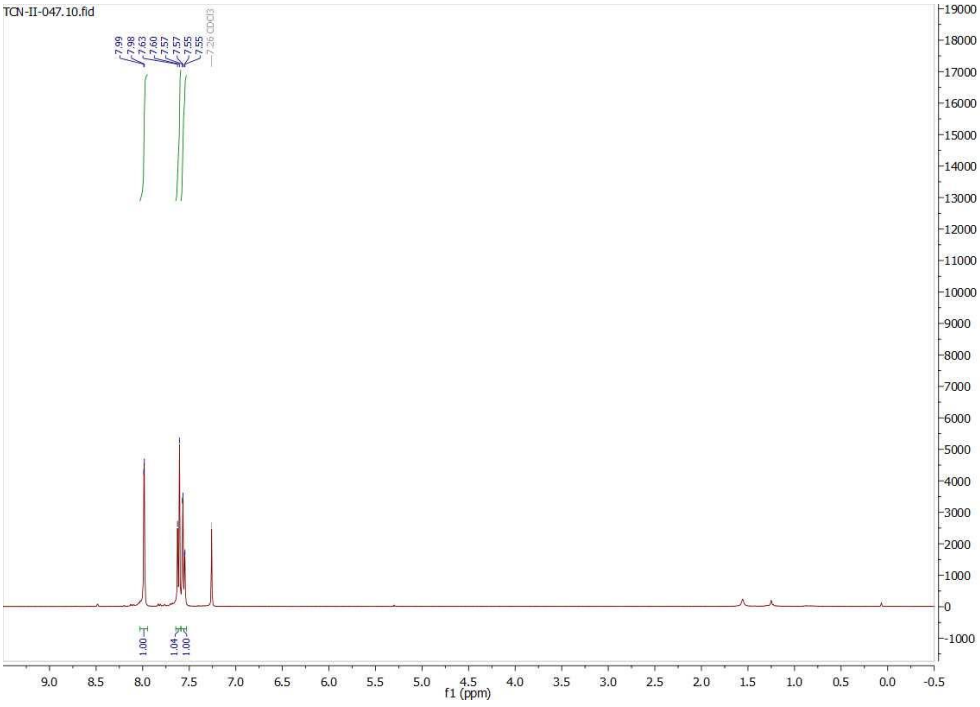

2C: 2'-nitro-[1,1':4',1"-terphenyl]-4,4"-dicarbaldehyde

NMR unavailable

3C: dimethyl 2'-nitro-[1,1':4',1"-terphenyl]-4,4"-dicarboxylate

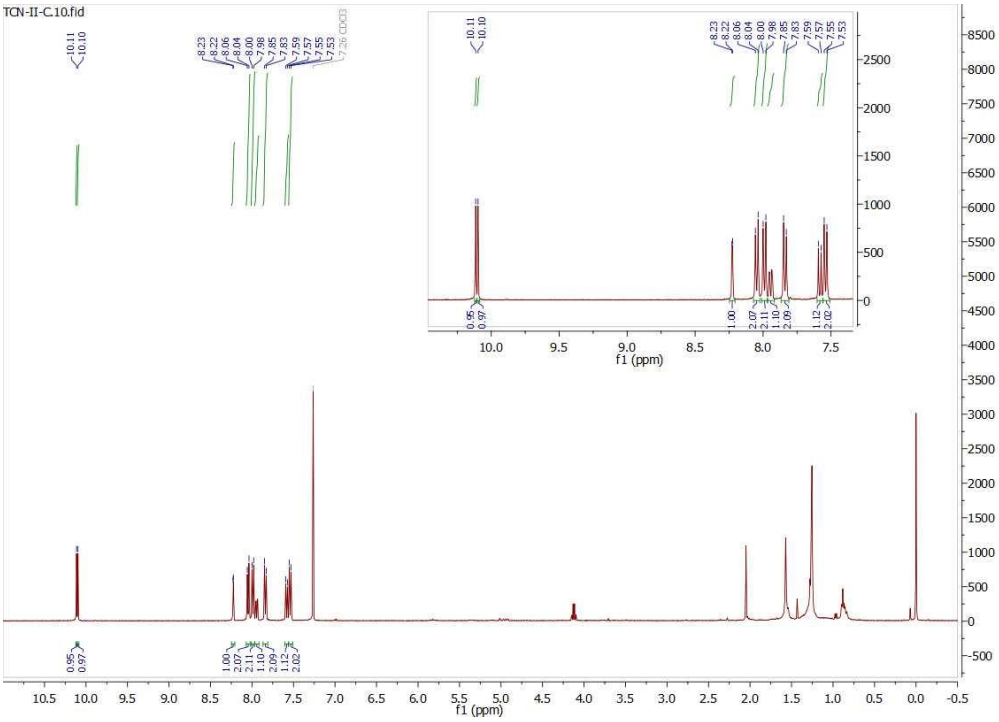

4C: dimethyl 2'-amino-[1,1':4',1"-terphenyl]-4,4"-dicarboxylate

NMR Unavailable

1D: 4,5-dimethoxy-2-nitrobenzaldehyde

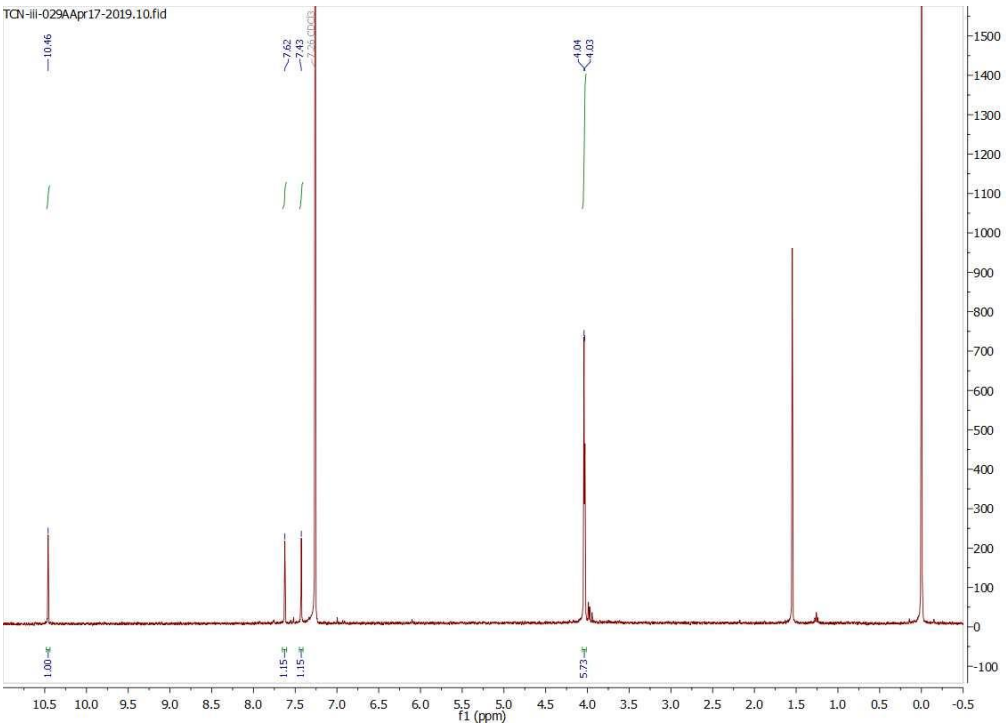

2D: (4,5-dimethoxy-2-nitrophenyl)methanol

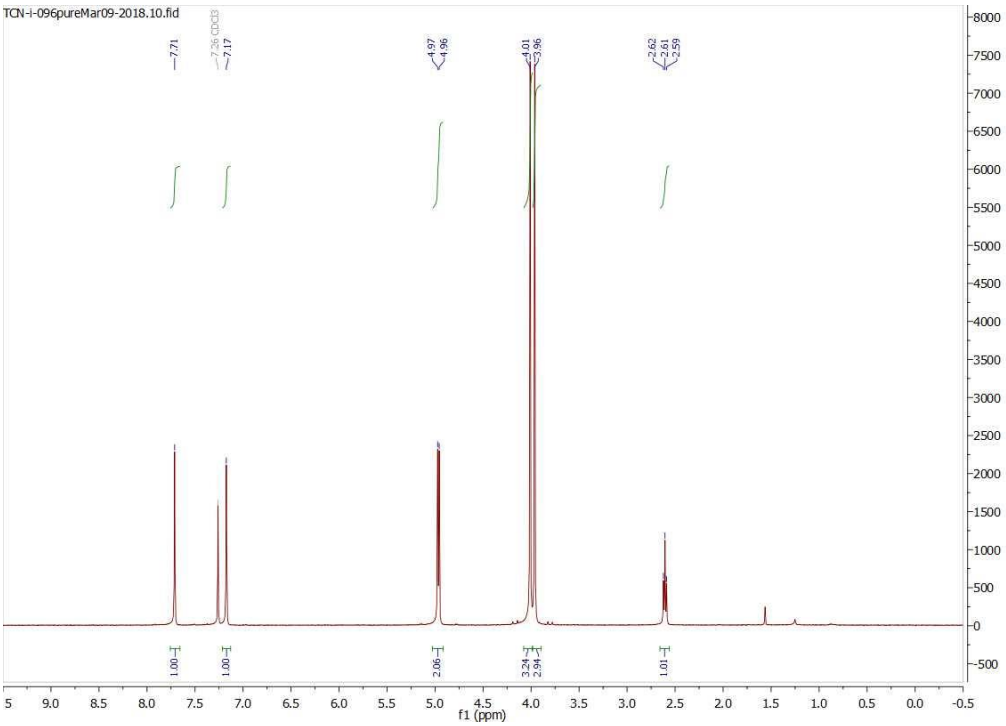

4D: dimethyl 2-((((4,5-dimethoxy-2-nitrobenzyl)oxy)carbonyl)oxy)-[1,1'-biphenyl]-4,4'-dicarboxylate

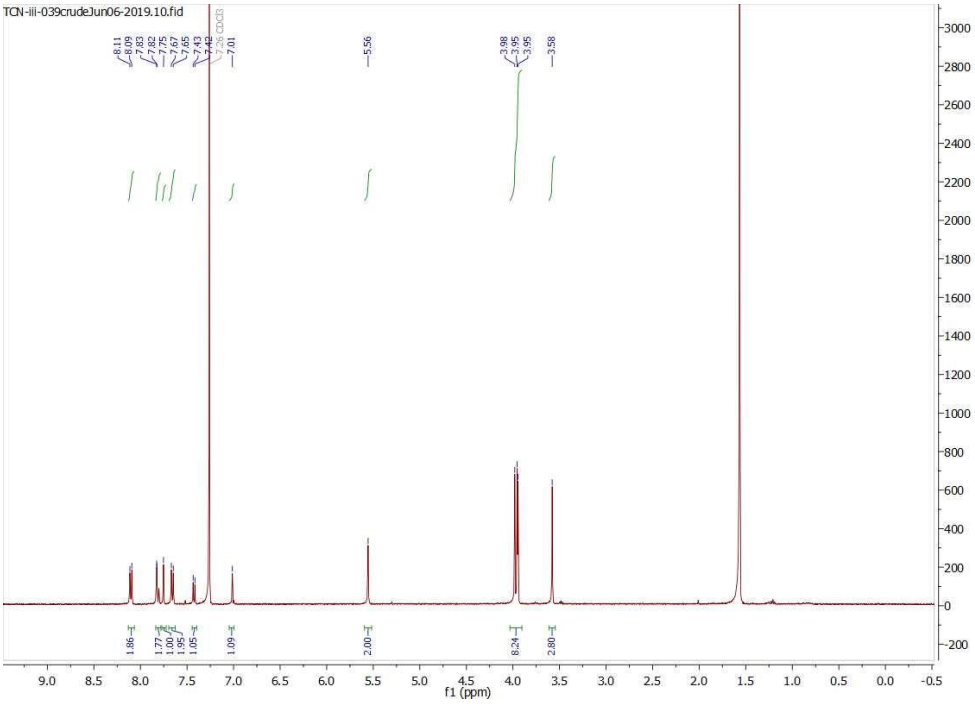

5D: dimethyl 2-((4,5-dimethoxy-2-nitrobenzyl)oxy)-[1,1'-biphenyl]-4,4'-dicarboxylate

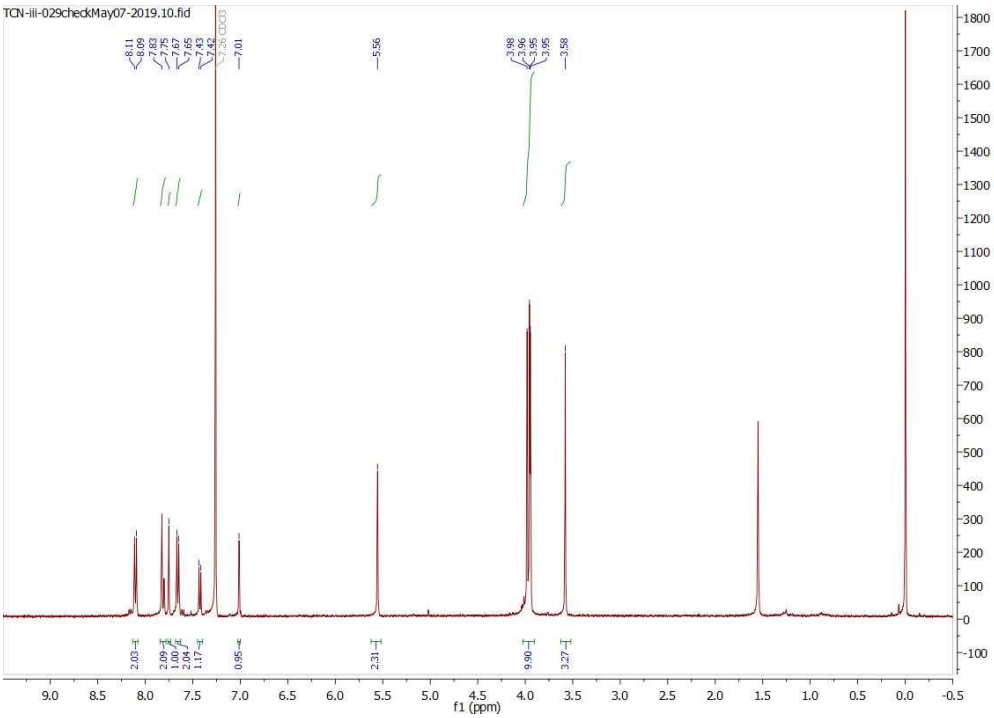

6D: 2-((4,5-dimethoxy-2-nitrobenzyl)oxy)-[1,1'-biphenyl]-4,4'-dicarboxylic acid

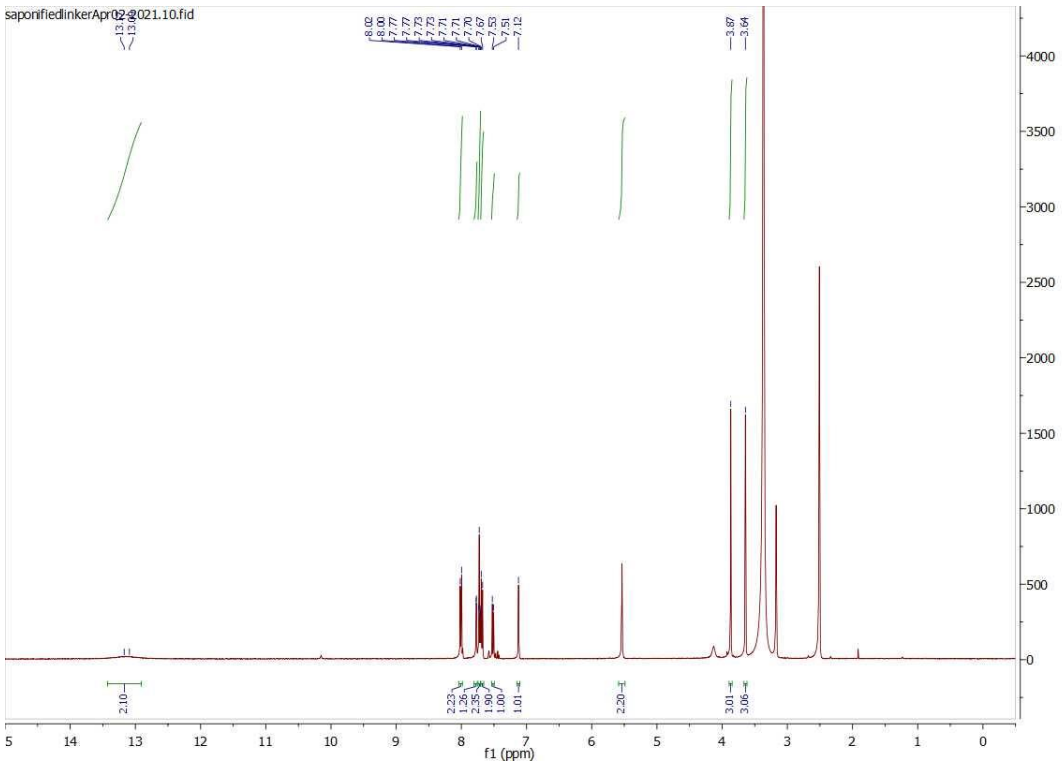

CHAPTER 6

MOF SYNTHESIS AND CHARACTERIZATION

6.1 Initial attempts at MOF synthesis

With completed linker in hand, it was time to begin synthesis of the proposed MOF material witch characterization in mind. Attempts began with conditions optimized for production of a single crystal x-ray diffraction quality material. It was initially assumed that single crystal XRD was the most effective source of structural confirmation and with limited knowledge of MOF synthesis, I began with this as my main goal. Many synthesis preparations within the primary literature list in detail how to produce material suitable for applying that material for the designed purpose, however there is limited information on how to optimize a synthesis for the goal of producing a single crystal for XRD. Discussion with our in-house crystallographer led to preparations that were more along to lines of growing single crystals from a solution of a single molecule in what I will call "slow recrystallization conditions". These conditions are effective for purifications or formation of single crystals of single compounds; however, they are and should be differentiated from conditions involving the *synthesis of two species*. Specifics of recrystallization conditions by and large prioritize the slow, even evaporation of the solvent in a static, open aired vessel and so this is where I began.

Initial MOF syntheses for my desired material involved the reaction between my MOF linker (1 equiv), zinc nitrate (4 equiv) and a high boiling point solvent such as

DMF, DEF and NMP (~ 1.0M solution of linker). After the dissolution of the zinc nitrate and MOF linker within the solvent, the open vessel was the placed into an oven at around 70 ºC. Many preps of zinc-based MOFs stated that MOF formation required between 3-5 days. However, under these conditions, all attempts were met with no solid MOF material and darkly colored solutions that were later indicative of deprotection of the o-NBE. It is well known that DMF under heated conditions (~90 ºC) decomposes to carbon monoxide and dimethylamine. At this point in the project, I believed that this process was acting as a disadvantage in my desired outcome, as I could envision a pathway where the produced dimethyl amine base was encouraging the deprotection of the linker. Later, I will describe how this was incorrect and that this pathway was actually advantageous in MOF formation. Incidentally however, at this point solvent conditions were altered to avoid the production of carbon monoxide and dimethylamine through the utilization of solvents such as DEF and NMP. These are solvents that are derivative of DMF and so should act similarly and have higher boiling points and thus discourage decomposition at the synthesis temperatures being utilized at this time. Despite the MOF formation attempts with DEF and NMP, the outcome of these syntheses were much the same as initial observations. In an attempt to discover solvents that may produce desirable results, other solvents screened include DMSO and ethylene glycol.

Following these failed syntheses, a collaborator from Georgia Tech University gave many helpful suggestions which greatly increased productivity. This collaboration provided much needed and beneficial guidance that led to more promising observations. Firstly, it was recommended to perform these reactions in high-pressure vessels that were able to heat high boiling point solvents at their boiling point or above. It was still

suggested to use static conditions, however it was made clear that closed conditions were best used in these cases, along with higher reaction temperatures. In addition to this, the recommendation of DMF as a solvent was surprising. However, it was explained that due to the decomposition of the solvent into dimethylamine, the produced base aided in the deprotonation of the carboxylic acid and thus in the chelation of the linker to the metal node. The two most important and impactful pieces of advice were 1) the most effective way to get a handle on MOF synthesis was to perform the procedure on a test substrate and 2) that zinc MOFs are notorious for their instability in the presence of any moisture in the solvent or air.

In learning that zinc MOF exhibit an instability to air moisture rationalized the failed attempts at synthesis in an open vessel. Heating solvent in an open vessel allowed for air moisture to enter the reaction system and thus inhibit reactivity. It also encouraged the usage of dry solvents which was a precaution previously untaken. In an attempt to understand this further, a computational study was found involving the association of water molecules with zinc nodes. It was observed in this study by Siegel and coworkers that the energy barrier of a water molecule insertion into the zinc node was competitive for the chelating energy of the linker carboxylic functionality once a sufficient number of water molecules are co-adsorbed to the zinc node. Specifically, it was calculated that one water molecule at the zinc node site endothermically could insert itself into the node at a ΔE=0.35 eV. However, once the number of water molecules was increased to four, the insertion because exothermic with a ΔE=-0.16 eV.[8]

In light of this study a choice was made to continue my MOF synthesis with zinc nodes with the aim at producing a robust proof of concept. Collaboration with Georgia

Tech resulted in adjustments made to my MOF syntheses that greatly encouraged me along to the road towards producing a material exhibiting the novel linker I had synthesized. The reaction test substrate of biphenyl-4 4'-dicarboxylic acid was chosen to match in similarity to the linker functionalized with the o-NBE gate. Initial test reactions were set up with this organic linker (1 equiv), zinc nitrate (1 equiv) and in DMF (0.01 M to linker) in a closed pressure vessel heating in the oven at either 85 or 90 ºC. It was discussed earlier the difference between *recrystallization* conditions and *synthesis* conditions. It was at this point in the project where the two concepts became distinct. My very first syntheses attempted to grow single MOF crystals via the slow evaporation of the solvent in which the components were placed. This strategy is most effective at the crystallization and purification of solutions that contain a single compound. However, formation of a MOF is a synthesis and not a recrystallization. A synthesis in this case is two separate compounds forming a combined new species and a recrystallization operate under different requirements. In an attempt to be brief, my initial MOF forming conditions were working against the goal of producing a single MOF crystal for XRD analysis.

Figure 16. Picture of solid MOF material clinging to the sides of the high-pressure vessel.

After revising my methodology on the test substrate, crystals presumed to be MOF material were observed for the first time during this project, seen in Figure 16. Modulation of the crystal size was able to be achieved with a slight variation in temperature. At 90 ºC or higher after four days, bulkier crystals were produced whereas at 85 ºC after seven days, smaller, more fine crystal were produced. Needless to say, the ability to presumably produce a MOF increased my

confidence in this area. Following these syntheses, characterization proved difficult. Many samples of what I observed to be single crystals were brough to the departmental crystallographer, however none of the samples were deemed adequate for XRD.

In an attempt to apply these optimized conditions to my MOF linker for the first time, the synthesis was applied to the gate-functionalized organic linker. The result of this reaction produced what appeared to be yellowish crystalline MOF material resembling closely what was obtained from the reaction of the test substrate. As previously observed the size of the crystals were able to be varied dependent on the temperature and time. Encouraged by this, many samples were brough to the crystallographer in an attempt to obtain structural data however out of many samples, only one batch was deemed suitable for an attempt at XRD. However, during preparation of the samples for XRD the moisture sensitivity of the zinc-based MOFs consequently deteriorated the sample sufficiently enough as to not allow for examination. One attempt was made to obtain a powder x-ray diffraction of a MOF sample in order to determine if my material was microcrystalline. Following PXRD analysis, it was observed that the samples I was producing were in fact not crystalline at the time of PXRD analysis but were amorphous in nature. My hypothesis surrounding this observation is that hydrolysis of the zinc nodes was playing a role in the deterioration of my produced MOF from the time of synthesis to the point at which a sample was prepared for analysis. Ultimately, the inhibition of characterization and structural elucidation seemed to be a result of sample preparation for data collection.

Determined to gain a better handle on the physical characteristics of the material I was producing, a collaboration with the Georgia Electron Microscopy (GEM) lab was

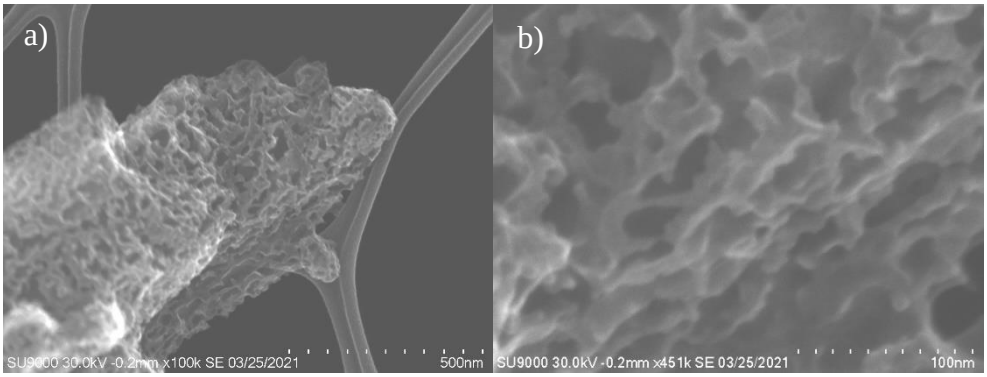

Figure 17. STEM images of the zinc MOF constructed from my gated organic linker. a) zoomed out, it is obvious to observe the overarching crystal features i.e., the broad faces of the particle and the hard edges at the corners. b) zoomed in it is clear that the surface of the particle appears pocked and carved out. It is theorized that is cavitation is due to hydrolysis of the zinc nodes at the surface of the particle.

formed. Transmission electron microscopy and scanning emission microscopy were able to be used in order to observe my samples in more detail. Supporting the suspicion that hydrolysis was playing a role in decomposition of my MOF, a scanning electron image of the surface of a zinc MOF crystal gave a much clearer picture. Observed in Figure 17, it can clearly be seen that while the overall structure of the crystal looks ordered, the surface has become pocked with cavities that have been carved away, suggesting that water hydrolysis has occurred at the surface of this material. This very helpful observation encouraged the utilization of a different metal within the node of the MOF primarily due to restrictions in the characterization.

6.2 Zirconium based MOF synthesis

It was at this point that the consideration to change to zirconium nodes was given more thought. Zirconium nodes have been largely explored and the MOFs derived from these metals have been tested under a wide variety of conditions. Zirconium based MOFs are well known for their robustness in aqueous conditions and even acidic conditions both at room temperature at elevated temperatures. Because of this, zirconium MOFs have been investigated greatly in biological applications and so for these reasons, my

MOF synthesis was adjusted. The new synthesis was changed to using zirconium chloride (1 equiv), my novel linker (1 equiv) and DMF as the solvent (5M solution to linker) in the closed pressure vessel system described previously. In addition to the optimized conditions a carboxylic acid modulator was required during zirconium MOF syntheses. Due to it being a stronger cationic metal, zirconium MOF formation occurs much more readily at higher temperatures and requires the implementation of mono carboxylic acid modulators. One advantageous result of this quick reaction is that the syntheses used for zirconium MOFs generally are completed within 24 hours.

Modulators, most often acetic or benzoic acid, during framework synthesis compete with the organic linkers for chelation of the metal nodes. The goal of modulator addition is to slow down the framework construction thus promoting larger crystal size and increasing overall crystallinity as well. In one study in 2011 by Behrens and coworkers', modulation of zirconium MOFs was investigated. In an un-modulated synthesis of zirconium chloride and both terephthalic acid (UiO-66) and biphenyl 4,4'-dicaroxylic acid (UiO-67), the slightly amorphous nanoparticles that were produced exhibited a diameter of ~50 nm. With an addition of either 10 or 30 equivalents of benzoic acid modulator respective to the quantity of linker, the nanoparticles grew, 100 nm and 200 nm in diameter respectively. Both of the modulated syntheses produced more unform crystals as well, as seen in Figure 18.[26]

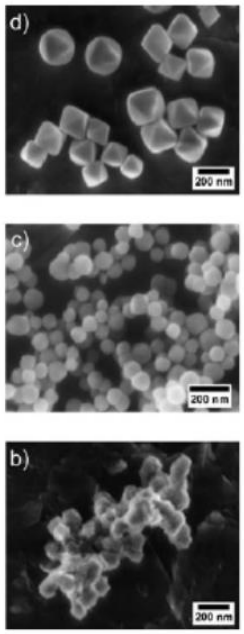

Figure 18. Example of how change in modulator equivalent changes overall size of MOF nanoparticles

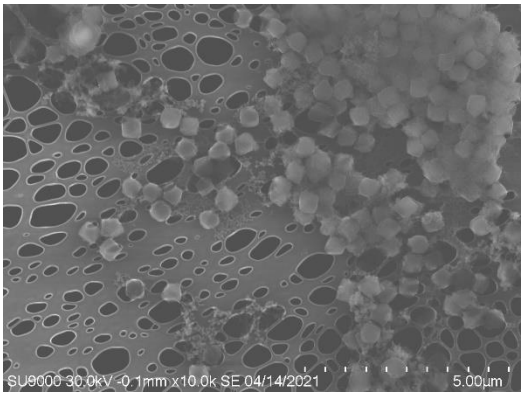

Figure 19. First zirconium-based MOF sample analyzed by the STEM at the Georgia electron microscopy lab. MOF particles that were produced exhibited much better apparent crystallinity and uniformity in both size and shape.

Considering modulation, higher temperature, reaction concentration as well as the other optimized conditions, my MOF linker was utilized in several syntheses varying only in the amount of modulator. In a typical synthesis, organic linker (25 mg) and zirconium chloride (12 mg) were both dissolved in 5 mL of DMF and then 10 - 30 equivalents of glacial acetic acid (30 – 90 µL) were added. The reaction vessel was sealed, wrapped in foil, and then placed in an oven at 125 ºC for 24 hours. The resulting off-white solid was centrifuged, the DMF was decanted and then replaced with fresh solvent (15 mL), and the MOF particles were resuspended for the centrifugation and rinsing steps to be repeated (x3). After three rinses with fresh DMF, the rinsing procedure was repeated with EtOH (x5) and then finally allowed to dry in an open vessel overnight. This procedure at first observation resulted in material that was much more robust as seen in Figure 19. Unlike the material of the zinc MOF, these crystals are not observed to have any cavitation on the surface, suggesting no hydrolysis due to moisture in the atmosphere or in the solvent

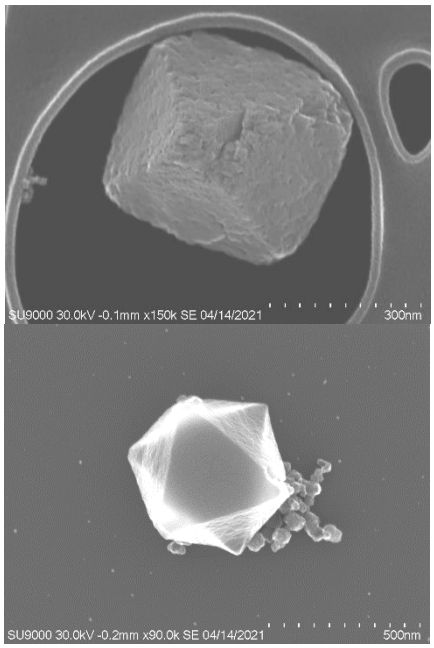

Figure 20. Change in modulator equivalents changing the particle geometry of the Zr based MOF constructed from my gate functionalized linker. a) 50 equivs of acetic acid produce MOF nanoparticle of the expected bipyramidal shape. b) 30 equivs of acetic acid produce MOF nanoparticles of unexpected icosahedron shape.

during synthesis. In regard to size modulation, it is difficult to make out differences in size at 30 or 50 equivalents of acetic acid modulator, primarily due to the change in particle geometry observed in using 30 equivalents of modulator. In previous syntheses with this organic linker, the typical bipyramidal particle geometry has been typical, however in the application of 30 equiv of acetic acid, an icosahedron shape is interestingly observed. It is unclear why the particle shape changes; however, it is intriguing to observe this difference while changing a variable designed to modulate particle size and not shape. SEM and TEM images are useful in the observance of the material on the surface level I was producing, however with the crystallinity of this material in question, selected area electron diffraction was attempted on all the samples produced. Unfortunately, these attempts were met with no diffraction observed. There are two possible reasons for this. The first and most obvious reason could be that my material was not crystalline in nature and was therefore amorphous. The second possibility is that the areas selected for the electron beam were too thick for the diffracted electron beam to be detected. In order to test and support the second hypothesis, a PXRD of this material would reveal whether or not this material is microcrystalline in nature or amorphous.

Following what was suggested to be a produced MOF material via STEM images, release of ibuprofen was tested via UV-Vis spectrometry. The loading of ibuprofen within the framework was accomplished *in situ*. A typical loading procedure included the optimized zirconium MOF synthesis condition mentioned above before, with the addition of 10 mg of ibuprofen.

CHAPTER 7

PHOTOLYSIS AND RELEASE STUDIES

7.1 Photolysis of diester liker precursor

In an attempt to gather data regarding the photolysis of the MOF after synthesis, o-NBE cleavage experiments were performed on the synthesized linker before saponification. This primary goal of this was the gain experience with the cleavage time and conditions necessary for the process to occur readily. Typical experiments for this process involved the dissolution of 10 mg of linker precursor in ~ 300 µL of $CDCl_3$ in an NMR tube. The sample of linker was irradiated over a 30-minute time period utilizing LED strip emitting UV light with a peak emission at 365nm. To observe photolysis, NMR analysis of the reaction was performed of the NMR tube reaction vessel t = 0min, t = 5min, t = 10min and t = 30minute time intervals. As seen in Figure 21, after 30 mins it was difficult to get specific peaks assigned to the product of photolysis, however tracking the consumption of starting material, the dissapearance of the "A" protons and the appearance of the "B" protons suggest the

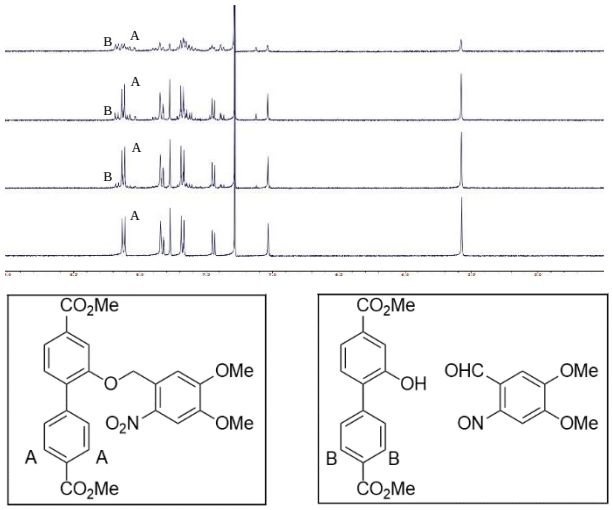

Figure 21. NMR experiment of the photolysis of the diester o-NBE functionalized organic linker backbone. Singlet peak at 5.5 ppm is the benzyl methylene carbon of the ether linkage and can be seen to decrease in intensity over time. Doublet at 8.1 ppm and the doublet appearing at 8.2 ppm after t0 can be used as references to the decreasing and increasing starting material and product, respectively. These doublets represent hydrogens A on the starting material and B on the product of photolysis.

predicted cleavage of the o-NBE. In order to test this in a completed MOF system, it was time to attempt the measurement of ibuprofen released following irradiation.

In order to test the release of ibuprofen, UV-Vis data was collected at certain time intervals during a period of exposure to 365 nm light. Before release studies were performed at certain time intervals, an ibuprofen calibration curve was constructed. Ibuprofen solutions of 0.008, 0.016, 0.032 0.049 and 0.065 mM were made and the absorbance of these solutions were recorded (Figure 22a). From this data, an standard ibuprofen calibration curve was made (Figure 22b) and from this a linear equartion was found. Following release studies, this linear equation was used to calculate concetration of ibuprofen solutions by reading the absorbance at 265nm. Following the construction of the calibratio curve, very preliminary release data in DI water was taken following a 10 second 365 nm light irradiation of gated MOF grown with 30 equivs of acetic acid. As seen in Figure 23a, the shoulder absorbance seen at ~265nm tracks similarly with the 0.032 mM standard ibuprofen absorbance superimposed

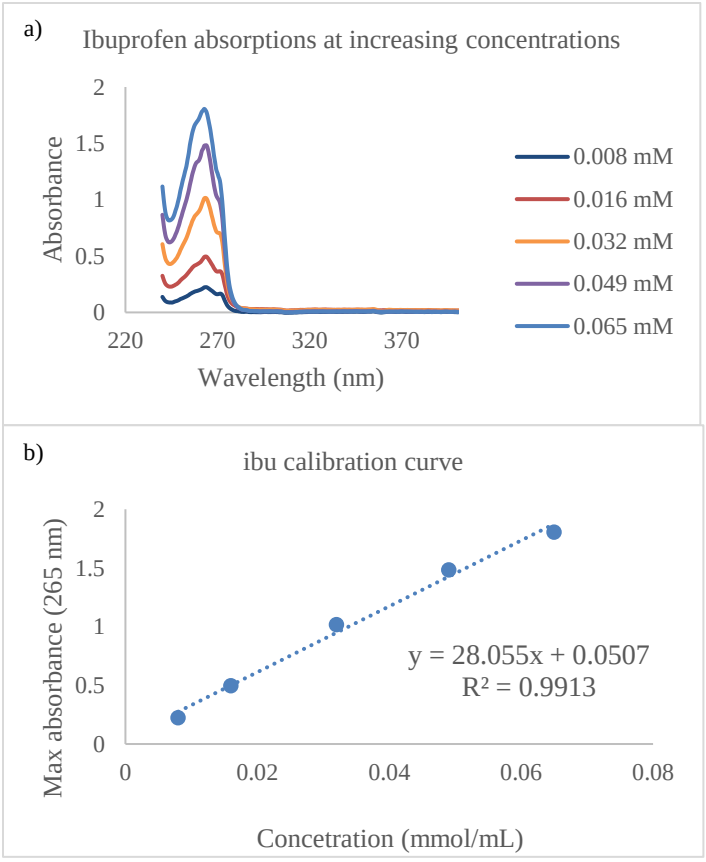

Figure 22. a) Ibuprofen calibration curve constructed by plotting max absorbance at 265 nm and concentration. R^2= 0.9913. b) Ibuprofen absorbances recorded at 0.008, 0.016, 0.032, 0.049 and 0.065 mM. Concentration curve was constructed by reading max absorbance at 265 nm.

underneath the experimental release absorbance data. This was encouraging data as it suggests the presence of ibuprofen after 10 seconds of irradiation of the gated MOF.

Following this observation, a more structured analysis was performed. For this, a stock solution of 30 equivalent acetic acid modulated gated MOF was prepared by suspension of a pipette tip of material in DI water. From this stock solution was pulled 0.500 mL for each ibuprofen release testing. Each 0.500 mL portion of stock solution was diluted in 2.5mL of DI water. The samples were irradiated at either 30 seconds, 1 min, 1.5 min, 2 min and 3 min. The absorbance for this release testing can be seen in Figure 23b. Consitent with the previous absorbance, a shoulder presumed to be ibuprofen is observed at 265 nm. For each run, the absorbance at this shoulder was recorded and then plugged into the linear equation obtained from the calibration curve. From this, the concetration of ibuprofen was calculated for each release test. These

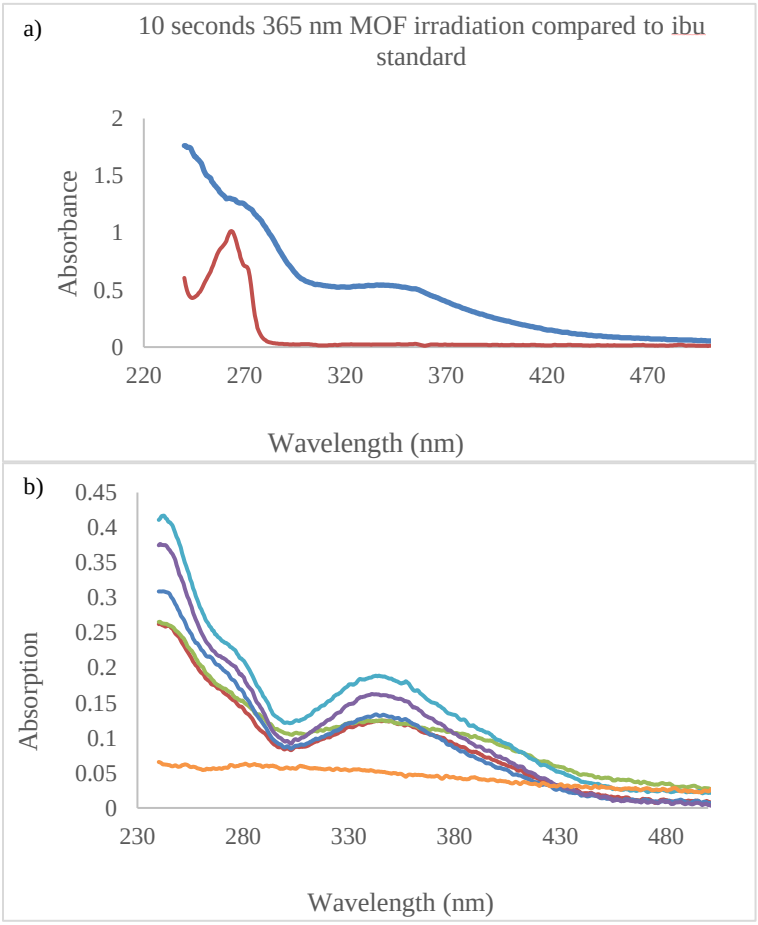

Figure 23. a) preliminary release study with standard ibuprofen absorbance (red curve) to compare against absorbance of gated MOF irradiated at 356 nm (blue curve). b) absorbances of gated MOF at the time intervals 30 sec, 1 min, 1.5 min, 2 min and 3 min. The bottom absorbance is absorbance following gated MOF suspension for 20 min in darkened conditions representing potentially residual cargo release within an aqueous media.

concetrations were then plotted versus time and the ibuprofen release curve, seen in Figure 24 was formed. If the absorbance utilized in these calculations is representative of the ibuprofen cargo, then it can be suggested that following longer intervals of irradiation at 365, ibuprofen concentration is increasing and thus being release from the MOF material.

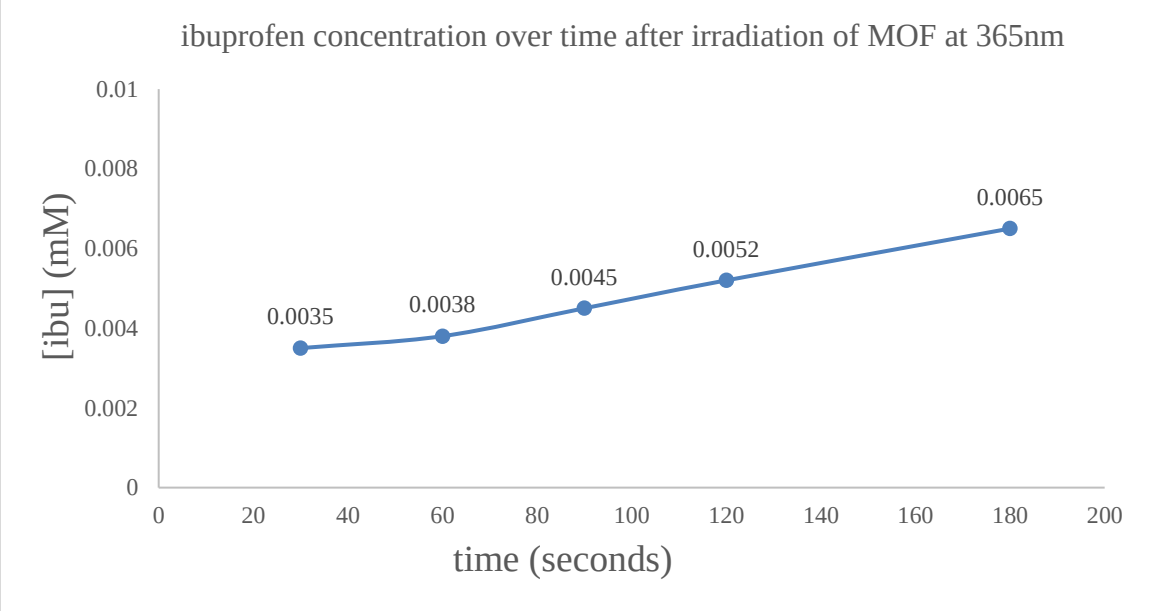

Figure 24. Increase of ibu concentration over time. Absorbance at 265 nm was taken and utilized to calculate the concentration of ibuprofen at varying time intervals. The time in seconds represents the time the gated MOF was irradiated at 365 nm light. An upwards trend in ibu concentration can be seen, suggesting a light dependent release of ibuprofen from the designed gated MOF.

In order to account for the nitrosobenzaldehyde photolysis product and gain a better understanding for if ibuprofen is being observed in in the UV-Vis data, absorbances were taken of irradiated unloaded gated MOF samples. The purpose of these experiments was to isolate the absorbance of the nitroso aldehyde and confirm the absence of the ibuprofen absorbance seen in these unloaded photolysis trials. Unloaded gated MOF samples were prepared in the manner described above and were irradiated at the 30 second, one, one and a half, two- and three-minute time intervals. As seen in Figure 25, an absorbance at 265 nm that is present in the loaded MOF photolysis

irradiation is unobserved in the unloaded experiments. This suggests that the absorbance at 265 nm is unrelated to the nitrosobenzaldehyde photolysis product, and suggests that it could be related to the ibuprofen cargo.

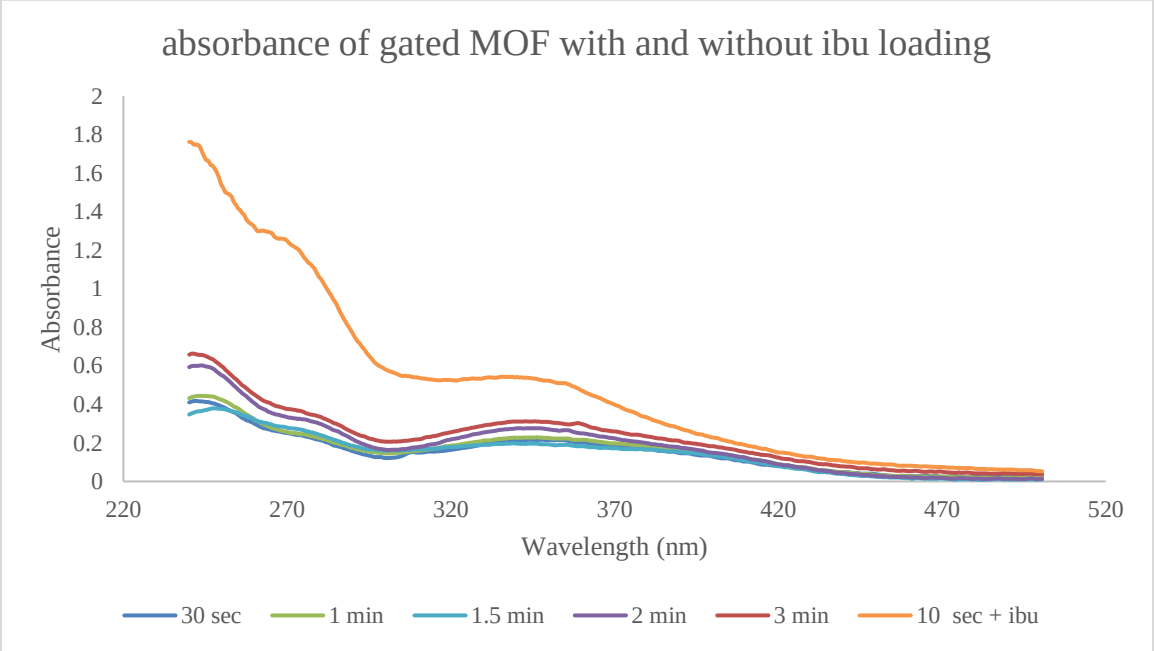

Figure 25. Comparison of empty gated MOF irradiated at different time intervals and ibuprofen charged MOF irradiated for 10 seconds. The drastic difference in absorbance is attributed to the greater quantity of MOF material utilized in the experiment. A clear shoulder in the ibuprofen loaded MOF absorbance at 265 nm is not observed in the time trials related to the unloaded MOF material. This suggests the should at 265 nm can be suggested as the ibuprofen absorbance. Absorbance at 345 nm at this point is attributed to the nitrosobenzaldehyde product of photolysis.

These release experiments are very preliminary and are being used to gain a foothold in gathering data for cargo release with my novel gated MOF. If these data support the specific, light controlled release of cargo, then more powerful modes of detection should be pursued. HPLC and GC/MS could be highly valuable in these attempts. HPLC will provide important quantitative data, directly relating to the amount of cargo being release with each irradiation. Using standard solutions of both the ibuprofen cargo and the nitrosobenzaldehyde photolysis product retention times for these

compounds should be found. Irradiation experiments should then be performed and the resulting supernatants tested for the presence of the cargo and photolysis product.

CHAPTER 8

IMPLICATIONS OF RESEARCH

If able to confirm structure through PXRD and analyze cargo release through more extensive studies, this MOF would be one of both novelty and innovation. Not only would this be the first attempt at developing a gated drug delivery MOF, but it would also confirm the plausibility of a system taking advantage of a release mechanism of this nature. Further advancements could be made in the area of drug delivery MOFs and other framework-based systems as well. Photo-labile moieties in addition to the o-NBE linkage could hold the potential to be applied to this design. It is my hope that as a result of this research, systems similar to this are developed that are more refined and have a wider range of applicability. Therefore, I regard the greatest implication of this research as furthering the advancement of not only drug delivery MOFs, but this area of chemical research in general.

Further reaching implications of course include the addition of this type of drug delivery system within the category of bio applicable materials. Discussed earlier in this dissertation, a distinction was made regarding the difference between drug delivery MOFs that operate through a passive release of cargo and through the reactive release of cargo. As a reminder, the framework of MOFs that passively diffuse their cargo from their pores either remain in-tact or disassemble through natural disassembly in the biological media. The advantages of a material that remains in-tact is that the components that comprise the framework are less impactful on its surrounding environment.

However, the drawbacks of a passive release are two-fold, 1) the release is generalized, non-specific and un-controllable and 2) the delivery times of these systems is sometimes on the order of five to six days. The delivery time here is less of a drawback than the delivery over time. In many cases and in the example presented by Férey et al., it has been observed that it may take six days to release 95-100% of the loaded cargo, however the bulk of the cargo (80-85%) is release within the first three days. In order to introduce consistency in the release, it could be suggested that a controllable release material is necessary.

In regard to stimuli dependent cargo release utilizing light as the stimuli, by and large the UiO-AZB MOF is employed. Described previously, this MOF utilizes the azobenzene linkage within the organic linker. The linker is isomerized from the E to Z isomer initiating the disassembly of the framework and subsequent cargo release. A compliment to this commonly investigated drug delivery system would be the MOF designed, developed, and synthesized herein. The ability to cargo release via light stimulation while retaining the overarching framework composition allows would be less impactful on the surrounding environment of the MOF. In this way, the qualities and benefits of a passive diffusion release MOF and the spatial and temporal control of a stimuli dependent MOF can come together in one material.

CHAPTER 9

SUMMARY AND CONCLUSIONS

As this section might imply some amount of completeness to this research project, it is my belief that there is yet much to do and many questions yet to answer to fully form the end of this project. Foundationally, much progress has been made since the first attempts at MOF linker design. Many iterations of drug delivery MOF linker were conceptualized and some of the syntheses for those were attempted- only one being completed. Through the syntheses that failed arose more refined and rationalized linker designs, however the failures were essential in the formation of these theorized systems. For example, from the inspiration of the failed pH functional cycloheptatriene linker, the photo-active gate functionalized o-NBE was designed and synthesized.

It should be reiterated that the successful synthesis of my target MOF is strongly supported in the visualization of the nanocrystals via STEM. While no specific area electron diffraction pattern was observed, the nanocrystals produced closely match those previously reported in the primary literature. Initial UV-Vis absorption experiments suggest that UV light has stimulated the release from the pores of the MOF, tracking the increase of absorption attributed to the ibuprofen cargo utilized. A way to probe this finding further would be to exchange the cargo that is being released. Many drug delivery MOF begin their release studies with either ibuprofen or caffeine. To increase the impact of the proposed drug delivery system as well as better gain an understanding on the delivery capacity of the MOF, 5-fluorouacil (5-FU) should be the next cargo of interest.

Exhibiting a very different absorption then ibuprofen (max absorption at 266nm)[27], 5-fluorouacil would also make a good candidate for testing due to its anti-cancer properties. Gathering data supporting release of (5-FU) would further suggest the application of this proof-of-concept MOF for eventual *in vitro* cancer cell viability assays.

While very initial release findings support the possibility of gate-opening assisted cargo release, many more experiments to further strengthen this support should be accomplished. Specifically, and probably the strongest evidence that would suggest release would be utilizing GC/MS or HPLC. In doing this, the quantification of cargo release would also be possible. GC/MS would allow for confirming the presence of the cargo outside of the framework and allow for the observation of whether the MOF framework itself is in disassembly during irradiation. A limitation of this GC study would be that these release experiments would have to be performed in organic solvents. Using reverse phase HPLC however would make cargo release studies possible in biomimetic aqueous solutions. In these experiments, the MOF would be tested within a phosphate buffer or other environment. Data relating to the quantity of drug delivery would be possible using HPLC as well.

Discussion of applying this material to *in vitro* cell viability assays must begin with the ability to prepare a nanoparticle (NP) for persistence within biological media. PEGylating the surface of nanoparticles enables them to relatively be masked to the hosts immune response. On top of this it also imparts colloidal stability of individual particles within an aqueous solution. Advantageous still, it enables the surface of the NPs to be decorated with targeting ligands specific to cell lines being tested. MOF nanoparticles are able to be PEGylated without further surface modification due to the exposed metals

nodes on their surface. It has been observed in the literature that amine terminated PEG chains are able to be chelated to the exposed zirconium sites on the surface of UiO-AZB.[27] In the future following PEGylation of the MOF surface, a targeting ligand specific to a cell line chosen for the *in vitro* cell viability assays should be ligated to the surface of the outer PEG shell, taking advantage of the terminal amine handle present at the end of PEG chains.

Proposed here are two future extrapolations of the synthesized gated drug delivery MOF that would greatly impact the possibilities this material may have in applications. These two proposed systems rely on both gold (AuNPs) and up conversion nanoparticles (UPCNPs). A sub-field that meshes both the MOF and nanoparticle fields is the investigation of so-called *nanoparticle@MOF nanohybrids*.[28] These relatively new materials possess combined traits that would otherwise be separated in two different materials, taking advantage of the optical, electrical, magnetic, and catalytic properties inherent to metal nanoparticles (MNPs) and applying these within MOFs that exhibit high inner surface area porosity. This class of nanohybrids being utilized multimodally, specifically for drug delivery, has been largely unexplored.

9.1 Gold nanoparticle with gated MOF shell

To this end, my hypothesis is that a material exhibiting the optical fluorescent capabilities of AuNPs and a highly porous outer MOF shell can be produced. It is first proposed that to obtain the MOF coating of AuNPs, a capping agent such as polydopamine can be used to functionalize the surface of the NPs. This method has been observed before in the primary literature[28a], and incorporates a handle by which MOF material is able to grow on the surface of nanoparticles. Following surface treatment of

the AuNPs with polydopamine, MOF growth, utilizing zirconium nodes and my designed organic linker, would then provide the NPs with a porous network allowing for the adsorption of drugs to be delivered. What makes this proposal pioneering is that both of the designed modalities (optical fluorescence and drug delivery) will function through the utilization of differing wavelengths of light. Selection of the core nanoparticle being AuNPs will allow for fluorescence that can be initiated by wavelengths within the range of 515-532nm. The optical fluorescence properties of AuNPs have been well documented[29] and will be utilized as a confirmational response that the drug delivery NPs arrive to the correct location within an *in vitro* assay. Once visual confirmation is suggested through fluorescence imaging made possible by the AuNP core, the release of biologically active small molecules can then be achieved through the utilization of 365 nm light. At this point, the UV light would open the gated MOF pores this allowing for drug delivery. A system as such could be defined as a "theranostic", a class of nanomaterials that involve the incorporation of both a therapeutic modality and a diagnostic modality. The ability to receive visual confirmation of nanoparticle uptake is valuable in the search for efficient

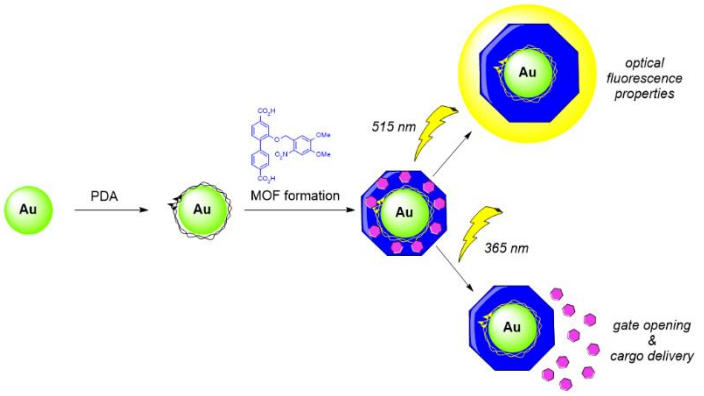

Figure 26. Theorized mode of utility for the proposed bimodal nanoparticle@MOF nanohybrid. The gold nanoparticle core, when irradiated at 515 nm, will emit optical fluorescence. The MOF material grown as the outer shell will provide the drug carrying porous framework and will be functionalized with the designed gated delivery MOF. At 365 nm irradiation, the pores will open and allow the cargo to be delivered. These two modalities used together will heighten the specificity of the drug delivery capabilities of this material, ensuring that the nanomedicine is in the correct location before administration of cargo.

drug delivery materials. Coupled then with the capacity for drug delivery, the proposed material could aid in the advancement of such nanomaterials.

9.2 UPCNPs

The final, and perhaps most impactful future direction for this novel MOF material could be argued to be the incorporation of it on to the surface of up conversion nanoparticles (see section 2.6). As discussed in the previous section, *nanoparticle@MOF nanohybrids* are a relatively new area of nanomaterials research, and to my knowledge, MOF coated UPCNPs have not been used in drug delivery to date. The most important argument against the utilization of my proposed MOF in drug delivery is the restricted skin penetration depth of the UV light necessary to initiate its drug delivery. As described before, lanthanide doped UPCNPs have the ability to modulate longer electromagnetic waves, such as IR frequencies into shorter wavelengths such as visible or UV wavelengths. To be applicable in this instance, a UPCNP that converts NIR wavelengths to UV wavelengths should be selected. NIR wavelengths have been observed to penetrate deeper into the skin, and therefore would be able reach the NP present at tumor sites at varying depths within the body. The proposal specifically would involve the coating of these UPCNPs with my designed MOF material, forming a novel *nanoparticle@MOF nanohybrid.* This nanohybrid would possess the ability to

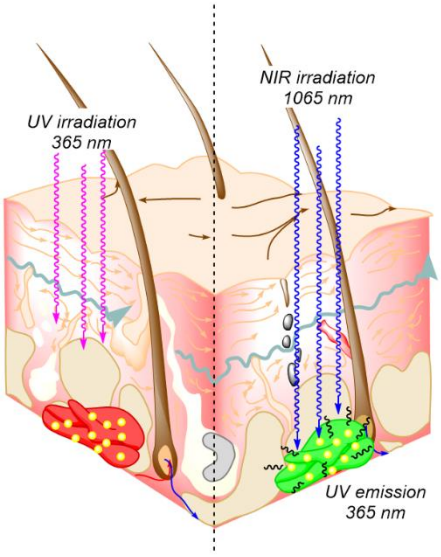

Figure 27. (Not to scale) relative depths of penetration for UV and NIR irradiation. A UPCNP coated in MOF material grown with my designed organic linker would be able activate drug delivery using wavelengths much more efficient in light stimulated therapeutics. In theory, the UPCNPs would have arrived at the tumor site via the EPR effect and upon NIR irradiation, those wavelengths would be converted to UV irradiation thus stimulating the gate opening of the MOF pores and subsequent drug delivery.

perform drug delivery at 365 nm wavelengths, however the source of this irradiation would be up-converted wavelengths emitted from the nanoparticle core of the nanohybrid. Therefore, this nanomedicine would possess the ability to instigate drug delivery through irradiation in the NIR window, visualized in Figure 27, enabling it to be reached at greater depths under the skin. This would also minimize any adverse effects of submitting biological tissue to UV light.

Ultimately, there is much potential in the novel MOF described by this research, both in and of itself, and also in application to nanomaterials. More thorough studies should be done in the analysis of drug release involving the framework itself, which would then lend itself to the usefulness of being integrated into other materials. However, a major driving force behind this research was its novelty and potential to impact the future of drug delivery MOFs. The possibility of my MOF being applied to biological systems is of course attractive, however the potential for this drug delivery system to be pioneering drove the intrigue equally. Seeking to be innovative, this project attempted to break the mold of what was observed to be typical in this subcategory of nanomaterials. As a contribution to the overall research surrounding MOFs, my greatest hope is that this project is representative of an example that strives for uniqueness. It has been my goal to allow this project to reflect the words of Dr. Omar Yaghi when he said "So, what are the limitations on this [MOF design]? The limitation in my opinion is really our own thinking."[1]

REFERENCES

1) Davenport, M. *Well, what are they good for, Omar?* [Podcast] *Stereo Chemistry*: February 28, 2018. Chemical and Engineering News. https://cen.acs.org/content/cen/articles/96/i10/Feast-ears-first-episode-new-podcast-stereo-chemistry.html

2) Yingwei Li and Ralph T. Yang. Gas Adsorption and Storage in Metal−Organic Framework MOF-177. *Langmuir* **2007** *23* (26), 12937-12944

3) Zoha H. Syed, Fanrui Sha, Xuan Zhang, David M. Kaphan, Massimiliano Delferro, and Omar K. Farha. Metal–Organic Framework Nodes as a Supporting Platform for Tailoring the Activity of Metal Catalysts. *ACS Catalysis* **2020** *10* (19), 11556-11566

4) National Cancer Institute. Clinical Trials Using MOF Compound RiMO-301. https://www.cancer.gov/about-cancer/treatment/clinical-trials/intervention/mof-compound-rimo-301. (Accessed July 6, 2021)

5) a) McKinlay, A., Morris, R., Horcajada, P., Férey, G., Gref, R., Couvreur, P. and Serre, C., BioMOFs: Metal–Organic Frameworks for Biological and Medical Applications. Angewandte Chemie International Edition, **2010** *49* (*36*): 6260-6266., b) Patricia Horcajada, Ruxandra Gref, Tarek Baati, Phoebe K. Allan, Guillaume Maurin, Patrick Couvreur, Gérard Férey, Russell E. Morris, and

Christian Serre. Metal-Organic Frameworks in Biomedicine. *Chemical Reviews* **2012** *112* (2), 1232-1268.

6) Daniel Bůžek, Jan Demel, and Kamil Lang. Zirconium Metal–Organic Framework UiO-66: Stability in an Aqueous Environment and Its Relevance for Organophosphate Degradation. *Inorganic Chemistry* **2018** *57* (22), 14290-14297.

7) a) Li, H., Eddaoudi, M., O'Keeffe, M. *et al.* Design and synthesis of an exceptionally stable and highly porous metal-organic framework. *Nature* **1999** 402, 276–279. b) Nathaniel L. Rosi, Juergen Eckert, Mohamed Eddaoudi, David T. Vodak, Jaheon Kim, Michael O'Keeffe, Omar M. Yaghi. Hydrogen Storage in Microporous Metal-Organic Frameworks. *Science*, **2003** *300 (5622)* 1127-1129. c) Steven S. Kaye, Anne Dailly, Omar M. Yaghi, and Jeffrey R. Long. Impact of Preparation and Handling on the Hydrogen Storage Properties of Zn4O(1,4-benzenedicarboxylate)3 (MOF-5). *Journal of the American Chemical Society* **2007** *129* (46), 14176-14177. d) Jaheon Kim, Banglin Chen, Theresa M. Reineke, Hailian Li, Mohamed Eddaoudi, David B. Moler, Michael O'Keeffe, and Omar M. Yaghi. Assembly of Metal−Organic Frameworks from Large Organic and Inorganic Secondary Building Units: New Examples and Simplifying Principles for Complex Structures. J*ournal of the American Chemical Society* **2001** *123* (34), 8239-8247.

8) Yang Ming, Nitin Kumar, and Donald J. Siegel. Water Adsorption and Insertion in MOF-5. *ACS Omega* **2017** *2* (8), 4921-4928.

9) Daniel Buzek, Slavomir Adamec, Kamil Lang, Jan Demel. Metal-Organic Frameworks *vs.* Buffers: case study of UiO-66 stability. *Inorganic Chemistry Frontiers.* **2021**., *8 (3)* 720-734.

10) Charity C. Epley, Kristina L. Roth, Shaoyang Lin, Spencer R. Ahrenholtz, Tijana Z. Grove, Amanda J. Morris. Cargo delivery on demand from photodegradeable MOF nano-cages. *Dalton Transcations*., **2017**, *46 (15)* 4917-4922.

11) Horcajada, P., Serre, C., Vallet-Regí, M., Sebban, M., Taulelle, F. and Férey, G. Metal–Organic Frameworks as Efficient Materials for Drug Delivery. **2006**. *Angewandte Chemie International Edition*, *45 (36)* 5974-5978.

12) Patricia Horcajada, Christian Serre, Guillaume Maurin, Naseem A. Ramsahye, Francisco Balas, María Vallet-Regí, Muriel Sebban, Francis Taulelle, and Gérard Férey. Flexible Porous Metal-Organic Frameworks for a Controlled Drug Delivery. *Journal of the American Chemical Society* **2008** *130* (21), 6774-6780.

13) C. Gaudin, D. Cunha, E. Ivanoff, P. Horcajada, G. Chevé, A. Yasri, O. Loget, C. Serre, G. Maurin. A Quantitative Structure Activity Relationship Approach to Probe the Influence of the Functionalization on the Drug Encapsulation of Porous Metal-Organic Frameworks. *Microporous and Mesoporous Materials.* **2012**. *157 (15)* 124-130.

14) Stuart R. Miller, Daniela Heurtaux, Tarek Baati, Patricia Horcajada, Jean-Marc Greneche, Christian Serre. Biodegradable therapeutic MOFs for the delivery of bioactive molecules. *Chemical Communications***, 2010,** *46 (25)* 4526-4528.

15) Schaate, A., Dühnen, S., Platz, G., Lilienthal, S., Schneider, A.M. and Behrens, P., A Novel Zr-Based Porous Coordination Polymer Containing Azobenzenedicarboxylate as a Linker. **2012** *European Journal of Inorganic Chemistry*, *2012 (5)* 790-796.

16) Shunjiro Nagata, Kenta Kokado, Kazuki Sada, Metal-Organic Framework tethered PNIPAM for ON-OFF controlled release in solution. *Chemical Communications*, **2015**, *51* (41) 8614-8617

17) Shunjiro Nagata, Kenta Kokado, Kazuki Sada. Metal-Organic Framework tethered pH and thermo-responsive polymer for ON-OFF controlled release of guest molecules. *Crystal Engineering Communications*, **2020**, *22 (6)* 1106-1111.

18) Cai, W., Wang, J., Chu, C., Chen, W., Wu, C., Liu, G. Metal-Organic Based Stimuli-Responsive Systems for Drug Delivery. *Advanced Science* **2019**, *6 (1)* 1801526.

19) Qiu, H.; Tan, M.; Ohulchanskyy, T.Y.; Lovell, J.F.; Chen, G. Recent Progress in Upconversion Photodynamic Therapy. *Nanomaterials* **2018**, *8 (5)* 344

20) Chase S Linsley and Benjamin M Wu. Recent advances in light-responsive on-demand drug-delivery systems. *Therapeutic Delivery* **2017** *8 (2)* 89-107

21) Malar A. Azagarsamy, Kristi S. Anseth. Wavelength Controlled Photocleavage for Orthogonal and Sequential Release of Multiple Proteins. *Angew Chem Int Ed Eng.* **2013** *52 (51)* 13803-13807.

22) a) Wenhao Shen, Jun Zheng, Zhansong Zhou, Dinglin Zhang. Approaches for the synthesis of o-nitrobenzyl and coumarin linkers for use in photocleavable biomaterials and bioconjugates and their biomedical applications. *Acta*

Biomaterialia. **2020**. *115 (1)* 75-91. b) Moon Suk Kim, Scott L. Diamond. Photocleavage of o-nitrobenzyl ether derivatives for rapid biomedical release applications. *Bioorganic & Medicinal Chemistry Letters.* **2006**, *16 (15)* 4007-4010.

23) Meng Wang, Gopal Abbineni, April Clevenger, Chuanbin Mao, Shukun Xu. Upconversion nanoparticles: synthesis, surface modification and biological applications. *Nanomedicine: Nanotechnology, Biology and Medicine*. **2011** *7 (6)* 710-729.

24) Shi Y, van der Meel R, Chen X, Lammers T. The EPR effect and beyond: Strategies to improve tumor targeting and cancer nanomedicine treatment efficacy. *Theranostics*. **2020** *25 10: (17)* 7921-7924.

25) Vlad Pascanu, Greco González Miera, A. Ken Inge, and Belén Martín-Matute. Metal–Organic Frameworks as Catalysts for Organic Synthesis: A Critical Perspective. *Journal of the American Chemical Society* **2019** *141 (18),* 7223-7234

26) Schaate, A., Roy, P., Godt, A., Lippke, J., Waltz, F., Wiebcke, M. and Behrens, P., Modulated Synthesis of Zr-Based Metal–Organic Frameworks: From Nano to Single Crystals. *Chem. Eur. J.*, **2011** 17 6643-6651.

27) Kristina Roth Stefaniak, Charity C. Epley, Joshua J. Novak, Margaret L. McAndrew, Hannah D. Cornell, Jie Zhu, Dylan K. McDaniel, Jennifer L. Davis, Irving C. Allen, Amanda J. Morris Tijana Z. Grove. Photo-trigered release of 5-fluorouacil from a MOF drug delivery vehicle. *Chemical Communications*. **2018**. *54 (55)* 7617-7620

28) a) Versatile Core-Shell Nanoparticle@Metal-Organic Framework Nanohybrids: Exploiting Mussel-Inspired Polydopamine for Tailored Structural Integration. *ACS Nano*, **2015**, *9* (7), 6951-6960. b) Surfactant-Directed Atomic to Mesoscale Alignment: Metal Nanocrystals Encased Individually in Single-Crystalline Porous Nanostructures, *Journal of the American Chemical Society* 2014 *136* (30), 10561-10564 c) Core–Shell Noble-Metal@Metal-Organic-Framework Nanoparticles with Highly Selective Sensing Property. *Angew. Chem., Int. Ed.* **2013**, 52, 3741–3745

29) Nonbleaching Fluorescence of Gold Nanoparticles and Its Applications in Cancer Cell Imaging. *Analytical Chemistry* **2008** *80* (15), 5951-5957